AD-A062 691 TEXAS TECH UNIV LUBBOCK DEPT OF CIVIL ENGINEERING F/G 1/3
DYNAMICS OF COMPLEX STRUCTURES-ANALYSIS AND EXPERIMENT: DAMAGED--ETC(U)
NOV 78 J H SMITH, W L BEASON AFOSR-77-3231

UNCLASSIFIED AFOSR-TR-78-1621 NL

OF
AD
A062891

END
DATE
FILMED
3-79
DDC

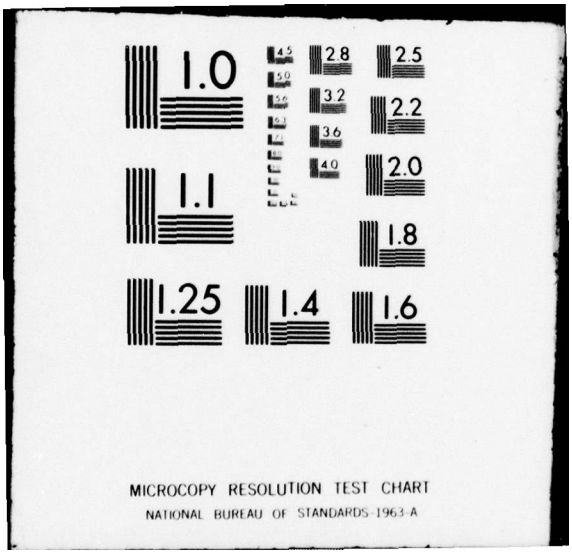
1.0
1.1
1.25
1.4
1.6
1.8
2.0
2.2
2.5
2.8
3.2
3.6
4.0
MICROCOPY RESOLUTION TEST CHART
NATIONAL BUREAU OF STANDARDS-1963-A

AFOSR-TR- 78-1621

DYNAMICS OF COMPLEX STRUCTURES- ANALYSIS AND EXPERIMENT: DAMAGED AIRCRAFT STABILATORS

by

JIMMY H. SMITH AND W. LYNN BEASON

FINAL REPORT

sponsored by

AIR FORCE OFFICE OF SCIENTIFIC RESEARCH
AIR FORCE SYSTEMS COMMAND, USAF

and

AIR FORCE ARMAMENT LABORATORY
VULNERABILITY ASSESSMENTS BRANCH
ADTC, USAF, EGLIN AFB, FLORIDA

under

GRANT NO. AFOSR 77-3231

TEXAS TECH UNIVERSITY

Lubbock, Texas 79409

NOVEMBER 1978

(6) DYNAMICS OF COMPLEX STRUCTURES-
ANALYSIS AND EXPERIMENT:
DAMAGED AIRCRAFT STABILATORS.

by

(10) Jimmy H. Smith [redacted] W. Lynn Beason

DEPARTMENT OF CIVIL ENGINEERING

TEXAS TECH UNIVERSITY

(9) Final Technical Report on Grant 15 Jan 77-15 Jul 78,
No. AFOSR 77-3231 from the
Air Force Office of Scientific Research
(15)

(18) AFOSR

(19) TR-78-1621

Lubbock, Texas

(11) Nov[redacted]78

(12) 88p.

409 832

FOREWORD

The research reported herein was co-sponsored by the Air Force Office of Scientific Research and the Air Force Armament Laboratory, Armament Development and Test Center (ADTC) under Grant No. AFOSR-77-3231.

The effort was begun 15 January 1977 and was completed 15 July 1978.

Listings of the computer program may be obtained from the authors or the Air Force Armament Laboratory (ADTC/DLYV), Eglin AFB, Florida.

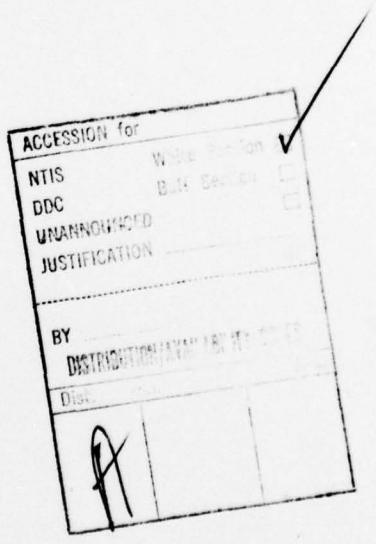

TABLE OF CONTENTS

LIST OF FIGURES

LIST OF TABLES

I. INTRODUCTION

Predictions of survivability and/or vulnerability of structures are complicated by any change in geometric or material descriptions. In particular, structures subjected to aerodynamic loadings may fail long before significant "strength" reduction (from induced damage) is inflicted. The current research is designed to study the various parameters that influence structural integrity of a stabilator and to develop a simplified method of predicting changes in certain structural properties as a function of damage level.

The overall objective of this research was to develop a static and dynamic response model for damaged horizontal stabilators. The project has been divided into three related tasks:

1. Conduct an experimental program on undamaged stabilator.
2. Develop a static and dynamic matrix structural analysis computer program which can be used to model stabilator response (both damaged and undamaged).
3. Develop a simplified response model for damaged stabilators which will allow quick, reasonably accurate estimates of the change in the stabilator's response (stiffness and fundamental frequency) as a function of damage.

Three types of tests were conducted on both damaged and undamaged stabilators: static tests, pluck tests, and forced vibration tests. The objectives of the experimental program were to determine: (1) the static deflection characteristics of the stabilators, (2) the stabilator's fundamental frequency and associated mode shape, and (3) as many other natural frequencies as practical.

The stabilators used in the experimental program were F3H type and were provided by the Air Force. A testing apparatus was constructed

to mount the stabilators in a vertical plane with loads applied horizontally. Instrumentation consisted of electronics displacement transducers dial gauges, geophones (velocity transducers) and accelerometers.

A series of tests were conducted on undamaged stabilators and on each of four damage locations as shown qualitatively in Figure I-1. A total of 60 tests were performed on the F3H stabilator.

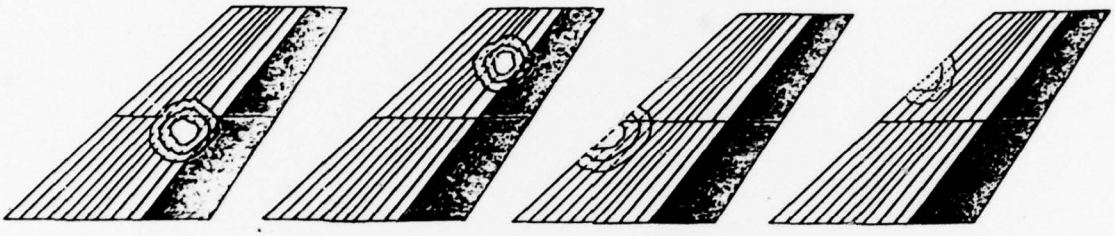

FIGURE I-1. DAMAGE LOCATIONS

The damage induced consisted of circular holes cut completely through both top and bottom skins and the internal members.

Although a test apparatus was also constructed to test A4 stabilators, only two tests were conducted before deciding that a complete test series on that particular stabilator was beyond the scope of this research effort.

A matrix structural analysis computer program has been developed to analytically model both the static and dynamic response of the stabilators. The basic element of the matrix formulation is a beam element which is capable of both bending and torsion. Each node of the system has three degrees-of-freedom: vertical displacement and two orthogonal rotations. The finished program employs a banded symmetric solution technique along with a Newmark-Beta technique for the dynamic analysis.

. The matrix structural analysis program described in more detail later can be used to give a complete description of the stabilator response to a given loading. In many cases, it is conceivable that an indication of the stabilator's fundamental frequency would be of use for a preliminary assessment of the effects of a particular type of damage. Therefore, a simplified model of stabilator response was developed to relate the fundamental frequency of a damaged stabilator to that of an undamaged stabilator. The method used provides reasonably accurate results for the F3H stabilator. The simplified response model is designed in such a way that it can readily be applied to various other stabilators.

II. ANALYTICAL TECHNIQUES

A primary objective of this research project is to develop a simplified method of analyzing the static and dynamic response of a complex structure, in particular an aircraft stabilator, which has been further complicated by various levels of damage and to do so with acceptable accuracy, reliability and convenience. Although some specialization of the analytical procedure to the particular structure investigated has been found desirable, the procedure and, in fact, the resulting computer program itself is capable of analyzing any two-dimensional surface subjected to out-of-plane loading. The method is limited to problems in which the structure being analyzed is either comprised of actual beam elements or can be idealized (or discretized) into one made of interconnected beam elements. Such modeling techniques have been proven effective for continuous metal plates (1), steel shells (2), and soil-covered concrete arches (3). Since the particular structure studied in this research was constructed primarily of identifiable structural sections, a transformation from a continuum to a grid system was not necessary.

A. Matrix Methods

The beam elements used in this development have six degrees-of-freedom with respect to absolute displacements of the nodes as shown in Figure II-1. These degrees-of-freedom are a vertical translation (Δ_z) and two rotations (θ_x and θ_y) at each end. The geometric position of the element is defined by the global coordinates of the end nodes (x_j, y_j, x_k, y_k) and the beam element is simply a straight line connecting the nodes. The essential properties of each element are the moment of inertia (I) about the principal axis parallel to the x-y plane, the polar moment

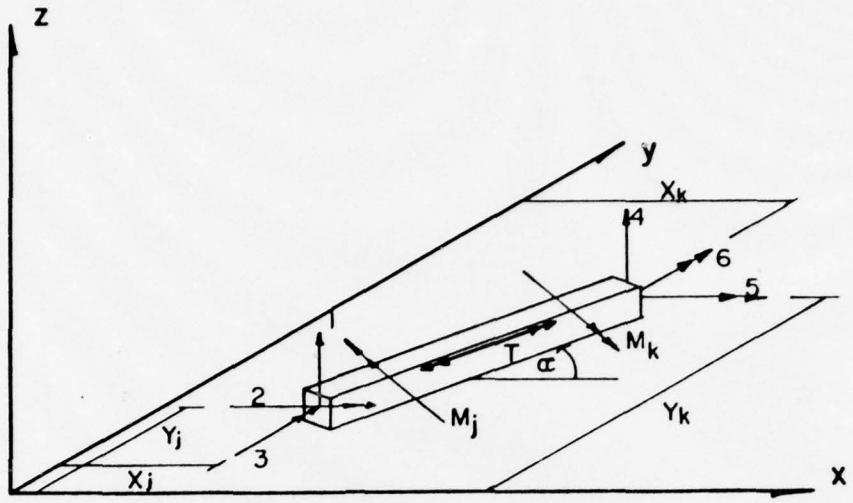

FIGURE II-1. BEAM ELEMENT NOMENCLATURE

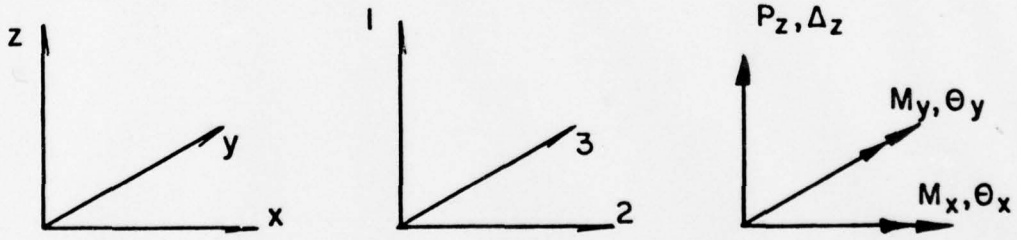

a) Positive Coordinates

b) Sequencing for Loading and Displacements

c) Force Deformation Notation

FIGURE II-2. SIGN CONVENTIONS AND NOTATION

of inertia (J), the modulus of elasticity (E) and the modulus of rigidity (G). Also noted in Figure II-1 are the predominate internal actions (forces) that result from nodal displacements. They are the moments about the principal axis at each end (M_j and M_k) and the torque (T).

In order to relate internal forces and deformations to nodal forces and displacements, a sign convention is necessary; Figure II-2 indicates the adopted sign convention for geometry (x, y, z) sequencing, and global forces (P and M) and displacements (Δ and θ).

Selecting the basic method of analysis was simple; the displacement method was chosen because it is ideally suited for both static and dynamic analyses. A description and derivation of the displacement method is unnecessary as it is widely used and published. However, the development of the stiffness matrix for the beam element used herein is somewhat unique in its simplicity and its adaptability to the particular type structure studied and, therefore, a complete development of this is presented.

First, it is known from the formulation of the displacement method that the external forces {f} are related to the external displacements {d} by the relationship:

$$\{f\} = [B]^T[k][B]\{d\} \tag{2.1}$$

and the internal forces {p} are determined by

$$\{p\} = [k][B]\{d\} \tag{2.2}$$

where B is a combination of compatibility requirements and a transformation from member to global coordinates and k represents the element stiffness matrix which contains the material and member properties. In this development, it is noted that for a single element:

$$\{f\} = \{P_{z_j} \quad M_{x_j} \quad M_{y_j} \quad P_{z_k} \quad M_{x_k} \quad M_{y_k}\}^T,$$

$$\{d\} = \{\Delta_{z_j} \quad \theta_{x_j} \quad \theta_{y_j} \quad \Delta_{z_k} \quad \theta_{x_k} \quad \theta_{y_k}\},$$

and $$\{p\} = \{M_j \quad M_k \quad T\}^T$$

The required element stiffness matrix in local coordinates is then:

$$[k] = \begin{bmatrix} \frac{4EI}{L} & \frac{-2EI}{L} & 0 \\ \frac{-2EI}{L} & \frac{4EI}{L} & 0 \\ 0 & 0 & \frac{JG}{L} \end{bmatrix}$$

If all displacements {d} except one are held at zero and the one given a unit value, there results internal deformations corresponding to the internal forces (M_j, M_k, and T), namely v_1, v_2, and v_3. Solving for these internal deformations yields one column of the compatibility/transformation matrix [B]. Continuing this procedure for all six external displacements results in:

$$[B] = \begin{bmatrix} -1/L & -\sin\alpha & \cos\alpha & 1/L & 0 & 0 \\ 1/L & 0 & 0 & -1/L & \sin\alpha & -\cos\alpha \\ 0 & -\cos\alpha & -\sin\alpha & 0 & \cos\alpha & \sin\alpha \end{bmatrix}$$

Assembly of all elements in a given structure and defining the global stiffness matrix [K] as

$$[K] = \Sigma[B]^T[k][B] \tag{2.3}$$

the following set of simultaneous equations are obtained

$$\{f\} = [K]\{d\} \tag{2.4}$$

which can be solved by numerous techniques. It is convenient that {K} is symmetric and if a proper numbering system for nodal point is chosen, it is also banded.

Other matrices that are required in a dynamic solution technique are the mass and damping matrices. The mass matrix for each beam element is formed using the lumped mass concept with half of the total mass considered lumped at each end and the rotational mass moment of inertia considered to be zero.

While the global damping matrix for dynamic response is more accurately formed as a linear combination of the global stiffness and mass matrices, experience in recent related studies by the investigators have indicated that a vector, and even a constant, for damping coefficients

results in far simpler calculational procedures with satisfactory results. Thus, this latter technique is employed herein.

When global stiffness, mass and damping matrices, and a corresponding applied force vector are assembled properly following the principles of the preceding section, the following matrix equation is established for dynamic response of the discrete element model.

$$[M]\{\ddot{u}\} + [C]\{\dot{u}\} + [K]\{u\} = \{F\} \tag{2.5}$$

Here [M], [C] and [K] are the mass, damping and stiffness matrices, respectively, $\{\ddot{u}\}$, $\{\dot{u}\}$, and {u} are the acceleration, velocity and displacement vectors, respectively, and {F} is the vector of applied forces. The mass and damping matrices are always constant in time, the stiffness matrix is constant with linear behavior, and the remaining quantities are all functions of time. For statics problems the first two terms drop out and either a single force vector is considered or load increments up to some final force vector are prescribed.

For static behavior a single solution of the matrix equation $[K]\{u\} = \{F\}$ is possible for linear structures. To carry this out, the stiffness matrix is first decomposed, and then back substitution is performed with the right-hand-side force vector. The computed displacements are printed out and may also be used in conjunction with the element stiffness matrices to determine the forces or stresses in individual elements.

For dynamic response problems, a direct step-by-step solution of the governing equations in time is employed. In this approach Equation (2.5) is applied over every time increment, dt, in order to determine the response quantities at the end of the interval (time t + dt) in terms of

the applied forces and the known quantities at the beginning of the interval (time t). At the end of the interval the equation may be written as

$$M\ddot{u}_{t+dt} + C\dot{u}_{t+dt} + ku_{t+dt} = F_{t+dt} \tag{2.6}$$

where the matrices M, C and K and the vectors $\ddot{u}$, $\dot{u}$, u and F are shown without brackets in the interest of brevity.

The generalized acceleration method developed by Newmark (Ref. 4) is used in a form that does not require iteration. The velocities and displacements at the end of a time increment (t+dt) are assumed to be related to the corresponding quanitities at the beginning of the increment as follows.

$$\dot{u}_{t+dt} = \dot{u}_t + [(1-\gamma)\ddot{u}_t + \gamma\ddot{u}_{t+dt}]dt$$

$$u_{t+dt} = \dot{u}_t + u_t dt + [(1/2-\beta)\ddot{u}_t + \beta\ddot{u}_{t+dt}](dt)^2 \tag{2.7}$$

Here γ is used as a weighting between the new and old accelerations in determining the new velocity, while β is a weighting factor between the same terms in determining the new displacement. Historically, γ has almost always been taken equal to one-half, but a variety of values of β have been used, depending on the order of the system (number of equations), the size of the time step and other factors. In particular, the stability and convergence of the method both depend upon γ and β. With $\gamma = 1/2$, a β value equal to or greater than one-fourth makes the method "unconditionally stable," that is, stable no matter how large

the time step is, and this is especially desirable for a system of large order. Then a time step need only be small enough to provide accuracy in the important lower modes of response; it need not be smaller than the shortest natural period in order to prevent instability. In this study γ is taken as one-half and β is taken as one-fourth in order to provide unconditional stability while keeping the mathematical damping as low as possible (Ref. 5).

If Equations (2.7) are substituted in Equation (2.6), all terms involving $\ddot{u}_{t+dt}$ are retained on the left-hand-side, and all other terms are gathered on the right-hand-side, then the equation to be solved at each time step becomes

$$\ddot{K}\,\ddot{u}_{t+dt} = \ddot{F}_{t+dt} \tag{2.8}$$

where

$$\ddot{k} = M + C[\tfrac{dt}{2}] + K[\beta(dt)^2] \tag{2.9}$$

and

$$\ddot{F} = F_{t+dt} - C[\dot{u}_t + \ddot{u}_t(\tfrac{dt}{2})] - K[\dot{u}_t + u_t(dt) + \ddot{u}_t(1/2-\beta)(dt)^2]. \tag{2.10}$$

Since the system remains linear and the time step dt is constant, $\ddot{K}$ needs to be decomposed only once, at the beginning of the time history. Then at each time step only back substitution is required (with the vector $\ddot{F}$, which changes from step-to-step because it depends on $\ddot{u}_t$, $\dot{u}_t$ and u_t) to find the new acceleration $\ddot{u}_{t+dt}$. The new values of velocity and displacement then are found from Equations (2.7).

B. Mathematical Model

To model the F3H stabilator a set of representative beam elements was devised based upon the geometry of the F3H stabilator. The F3H stabilator consists of a set of channel sections and a honeycomb stiffner "wrapped" in a thin metal sheeting. The interior construction of one of the F3H stabilators was exposed by partially removing the thin metal sheeting from one side of the stabilator. Measurements and observations taken from this stabilator were used to calculate the cross-sectional properties of the representative beams.

The surface of the F3H stabilator was divided into 161 strategically located node points (Figure II-3). A set of 290 beams were selected such that all of the stabilator channel sections acting in the longitudinal direction along with all of the thin metal sheeting was accounted for by model longitudinal beams and, further, so that all of the stabilator channel sections acting in the transverse direction and all of the metal sheeting was accounted for by model transverse beams. The centerlines of the 290 model beams are also shown in Figure II-3.

The cross-section of a typical stabilator model beam of width w consisted of a channel section of depth, d, with legs of the length, b, and uniform thickness, t_c, with a thin metal sheeting of thickness, t_t, attached to the top flange of the channel and a thin metal sheeting, t_b, attached to the bottom flange of the channel (Figure II-4). Three cross-sectional properties were calculated for each beam: the cross-sectional area, the moment of inertia of the cross-section, and an approximate value of the torsional rigidity of the section. The depth of the stabilator continually varies in each direction so that the equivalent model beams had to be devised. To determine the properties of the equivalent beams,

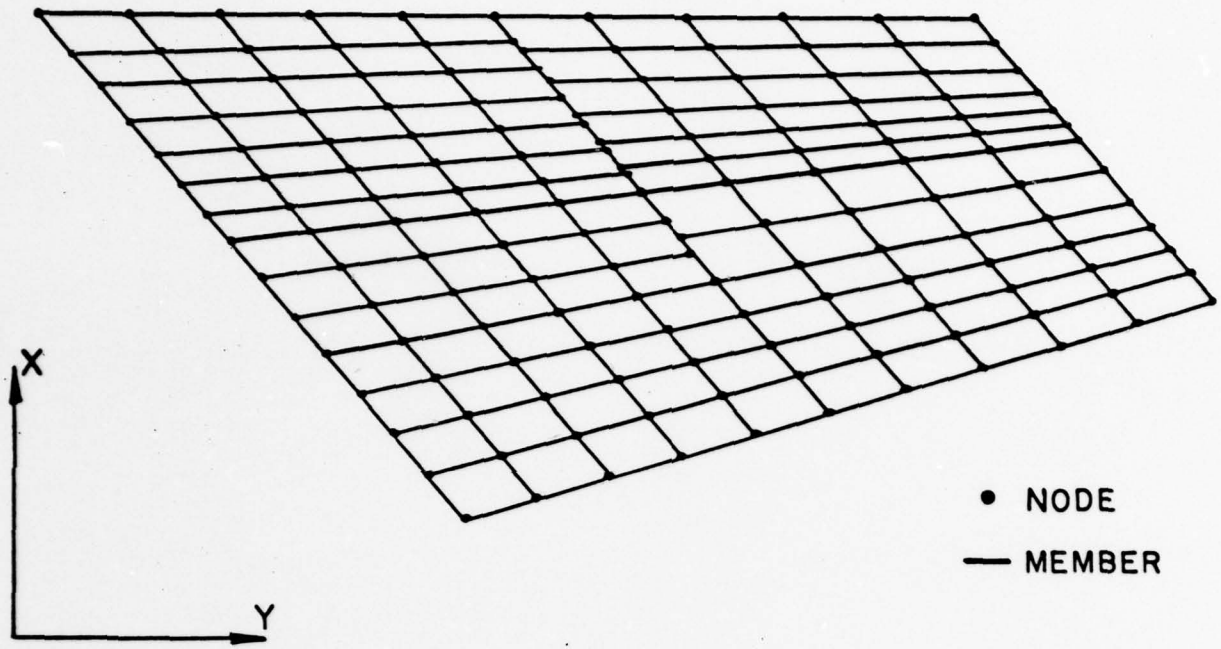

FIGURE II-3. SCHEMATIC OF F3H MATHEMATICAL MODEL

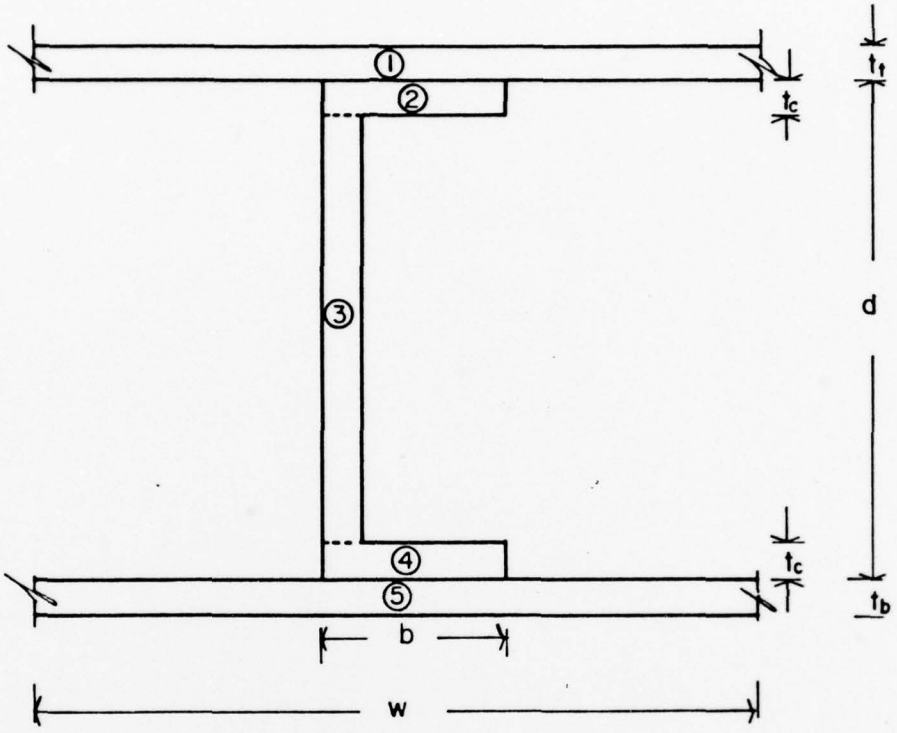

FIGURE II-4. IDEALIZED STABILATOR MEMBER

the three cross-sectional properties were calculated at each end of the stabilator beams and an average of the properties at both ends was considered to act throughout the length of the beam.

The idealized beam sections were typically divided into five simple rectangular sections as shown in Figure II-4. First, the total area of the cross-section, A_o, was calculated by summing the area of the individual cross-sections as

$$A_o = \sum_{i=1}^{5} \left[a_i\right] \tag{2.11}$$

where a_i represents the area of the i^{th} rectangular area. The neutral axis of the cross-section was located in the usual manner as follows:

$$\bar{y} = \sum_{i=1}^{5} \left[a_i y_i\right] \Big/ A_o \tag{2.12}$$

where y_i is the vertical distance from the bottom extreme fibers of the cross-section to the centroid of the i^{th} rectangular section. Then the moment of inertia of the cross-section, I_b, was determined using the parallel axis theorem as follows:

$$I_b = \sum_{i=1}^{5} \left[\frac{1}{12} b_i h_i^3 + a_i\ (y_i - \bar{y})^2\right] \tag{2.13}$$

where b_i and h_i are the width and height of the i^{th} rectangular section respectively, Finally, a value for the torsional rigidity (J) of each stabilator beam section was approximated (Ref. 6) as follows:

$$J = [4(A_s)^2] \; / \; \Sigma(l_i/t_i) \tag{2.14}$$

where l_i represents the larger dimension of the i^{th} rectangle, t_i represents the smaller dimension of the i^{th} rectangle, and A_s is the open rectangular area of the idealized beam.

Based upon trends observed in the experimental phase of this research it seemed reasonable to model nominal damage to the F3H stabilator by simply modifying all of the cross-sectional properties of the model beams in the area of the damage by a linear factor depending upon the percentage of the theoretical beam surface removed by the postulated damage. Such a procedure to model stabilator damage is admittedly an approximation to the real case; the choice of the linear factors used to model a particular level of damage was somewhat dependent upon engineering judgment.

C. Frequency Analysis

It is a well-founded concept in structural dynamics that the time variant displacement in a given direction z(t, x, y) at a particular point on a structure can be expressed as the summation of different modal components as follows

$$z(t, x, y) = \sum_{i=1}^{n} A_n(t) \; \phi_n(x, y) \tag{2.15}$$

where $A_n(t)$ is the modal displacement amplitude and $\phi(x, y)$ is the characteristic shape function. The characteristic shape functions, $\phi_n(x, y)$,

must all be orthorgonal for modal analysis to be valid (Ref. 7). The variation of the modal displacement components, $A_n(t).\phi_n(x, y)$, are periodic and for an undamped system they are considered to be of the following form

$$A_n(t).\phi_n(x, y) = \alpha_n \cos\omega_n t + \beta_n \sin\omega_n t \qquad (2.16)$$

where α_n and β_n are displacement amplitude constants for the n^{th} characteristic shape and ω_n is the circular frequency associated with the n^{th} characteristic shape.

Output from the computer program consists of discrete values of $z(t, x, y)$ for different locations on the F3H stabilator. To estimate the displacement amplitude constants and the circular frequency associated with the first several characteristic shapes, a forward selection nonlinear least squares regression technique was employed. Best estimates for the modal coefficients, α_n, β_n, and ω_n were found for the first several modes such that the undamped deflection function, $z(t, x, y)$, output from the computer program could be represented as follows:

$$z(t, x, y) = \bar{z} + \sum_{n=1}^{N} [\alpha_n \mathrm{COS}\alpha_n t + \beta_n \sin\alpha_n t] + \varepsilon_t \qquad (2.17)$$

where $\bar{z}$ is the mean nodal deflection, N is the total number of modal amplitude functions considered, and ε_t is the error present at time t. The mechanics of least square regression are not discussed herein as the subject is well treated elsewhere (Ref. 8).

To define the characteristic stabilator shape $\phi(x, y)$ associated with a given node, the regression procedure was applied to several different node points along the surface of the stabilator. While the displacements

at different node points experience different relative magnitudes of modal contributions, each point generally experiences significant contributions from the same circular frequencies and the modal contributions of the common circular frequencies at different node points are in phase. Further, the modal displacements amplitude, $A_n(t)$, is independent of the node location. Therefore, the relative magnitudes of the vertical deflections, $z(t_o, x, y)$, at different node points along the stabilator taken at a given time, t_o, define the characteristic shape of the stabilator. In this manner, the different characteristic shapes can be defined as precisely as warranted from the computer output.

III. TEST SPECIMENS AND APPARATUS

The tests described herein were conducted in the structural testing laboratory of the Department of Civil Engineering, Texas Tech University. The test specimens were provided by the Air Force Armament Laboratory (AFATL), Eglin AFB, Florida. Most of the testing apparatus was already available; however, the Ling shaker and amplifier were borrowed from AFATL and the digital graphic system for data interpretration was purchased during the course of the research. In order to document all aspects of the program, details are presented in the following sections on the specimens tested, the support system to hold them, the loading systems employed to impose loads and deflections, and the measuring system used to record the response. The procedures and results are presented in Chapter IV.

A. Test Specimens

A total of six horizontal stabilators from F3H aircraft were available for testing. One was disassembled, i.e., the skin removed, to provide geometric information such as skin thicknesses, internal member sizes, and amount of honeycomb material (shaded in figure) inside. This information was necessary for subsequent computer data development; documentation is in a subsequent chapter and will not be duplicated here. Figure III-1 shows the method that was used to inflict damage on the stabilator.

Four of the specimens were subjected to a series of static and dynamic loads and one was retained intact in case the investigators or the Air Force later desired testing of a different nature.

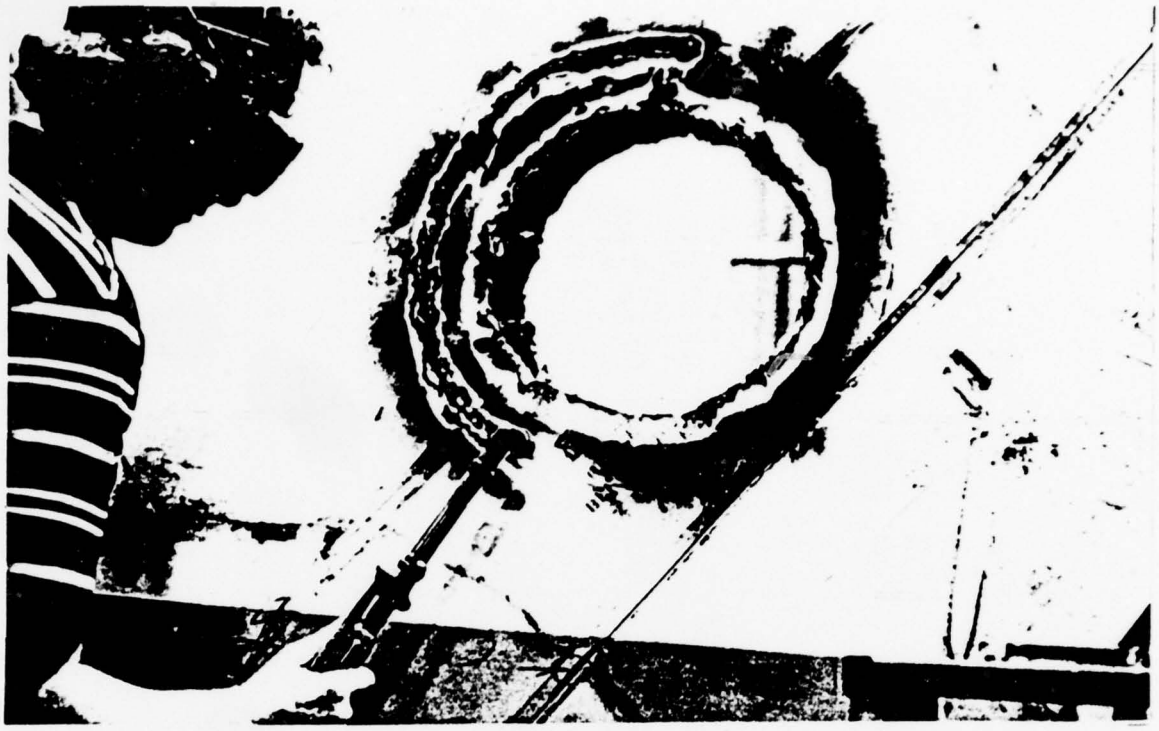

a) Interior Damage

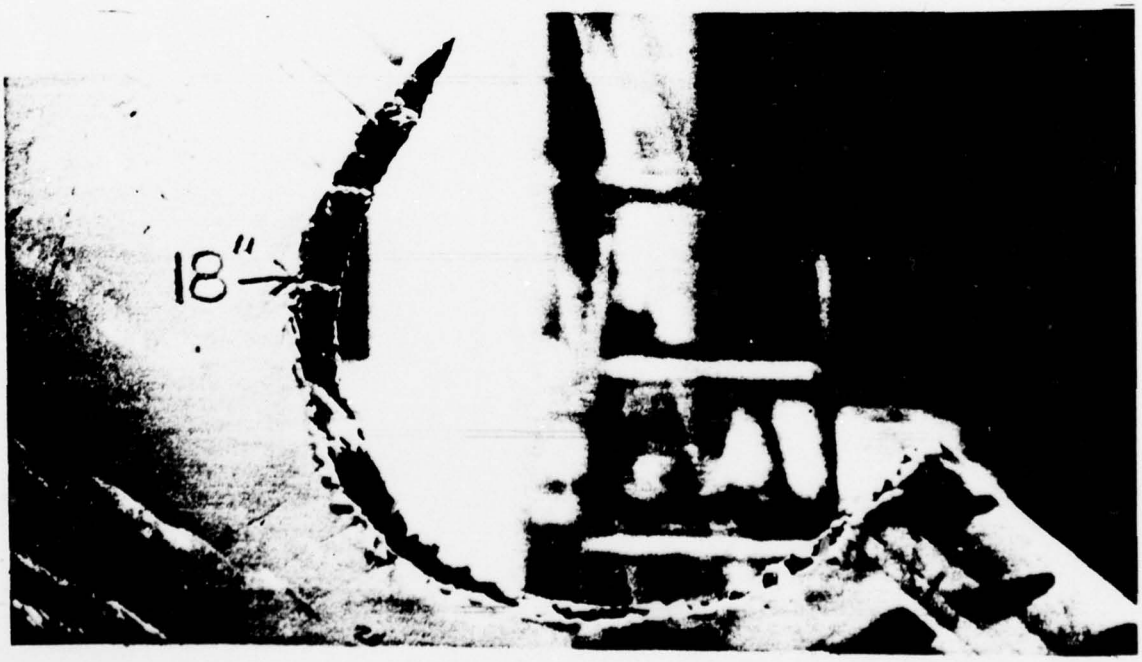

b) Leading Edge Damage

FIGURE III-1. EXAMPLES OF DAMAGE

B. Test Apparatus

An overall view of the test arrangement is shown in Figure III-2; each component will be discussed separately. The support system for anchoring the stabilators consisted of an extremely rigid frame constructed of steel. Total weight of the test frame was approximately 1000 lbs. The primary function of the test frame was to rigidly transfer the loads from the stabilator to the reinforced concrete test deck. The test frame was attached to the 2-ft thick concrete test deck using five 2-inch diameter high strength bolts. Figure III-3 shows a side and end view of the anchoring frame and clamping system. The frame itself is considered infinitely rigid for all practical purposes, but some flexibility was inherent in the clamping device because it had to be designed so that several different stabilators could be installed and removed with relative ease.

Static loads were applied to the test specimens by servo-controlled hydraulic rams, which were electronically controlled from the panel shown in Figure III-4. Dynamic loads were applied by two methods as indicated in Figure III-5. For forced vibrations, a Ling shaker with a sine-wave signal generator and amplifier was employed. Initially, the hydraulic UEH dynamic actuators were tried, but it was determined that the Ling electronic shakers provided a greater range of frequencies and more accurate controls and was, therefore, more appropriate for the type of tests being conducted. For impact loads, a "pluck" test was performed in which the specimen was subjected to a static force by means of a steel wire (1/8 in. diameter) attached to a hydraulic actuator. The static load was then released suddenly by cutting the steel wire, allowing the specimen to vibrate freely. This induced a vibration which was free of any added mass, allowing the first fundamental frequency and damping to be accurately observed.

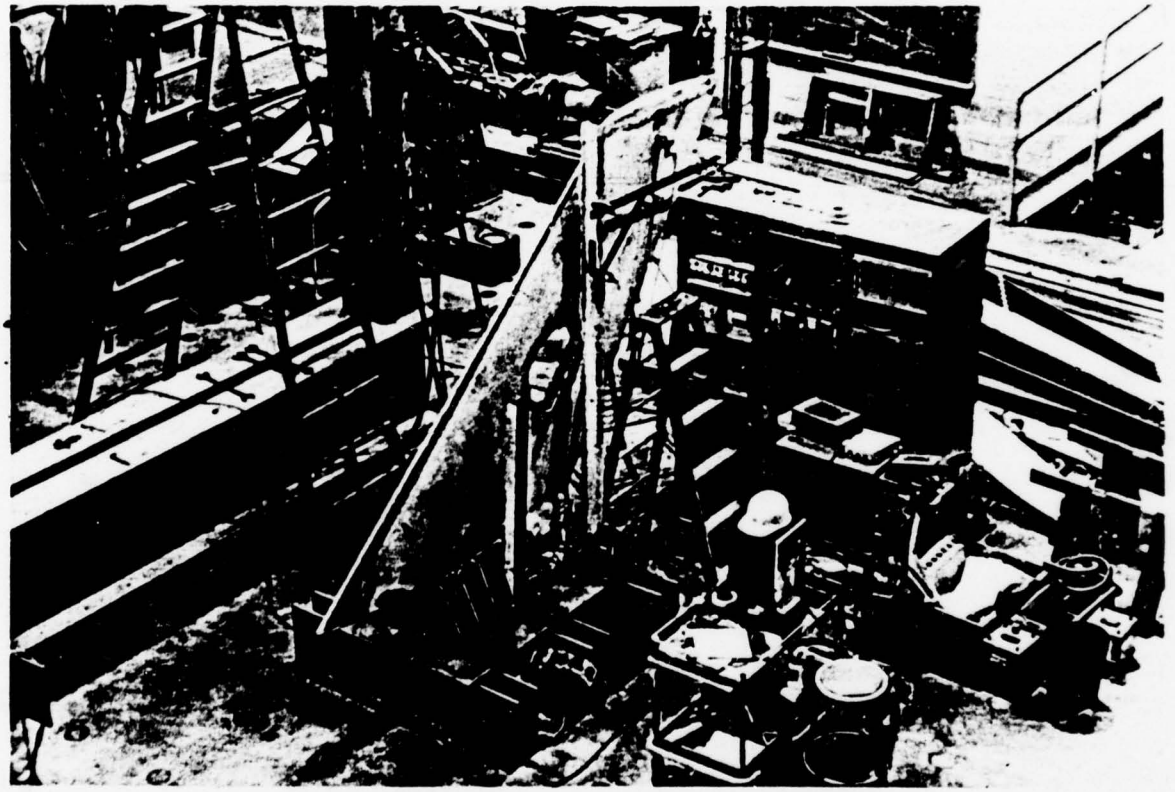

FIGURE III-2. OVERALL VIEW OF TESTING ARRANGEMENT

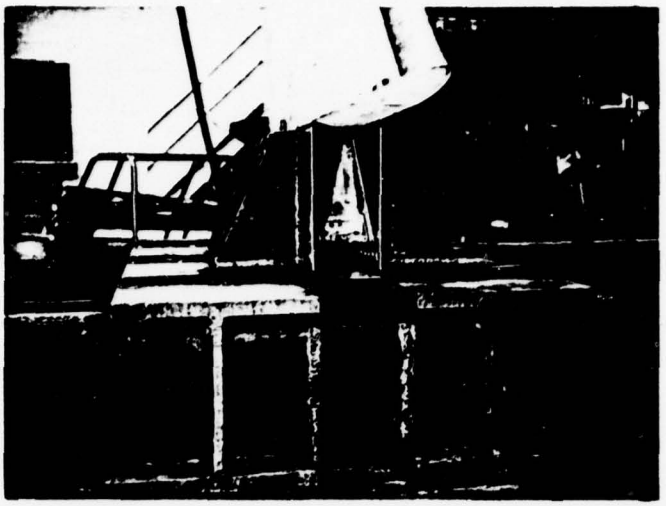

a) End View

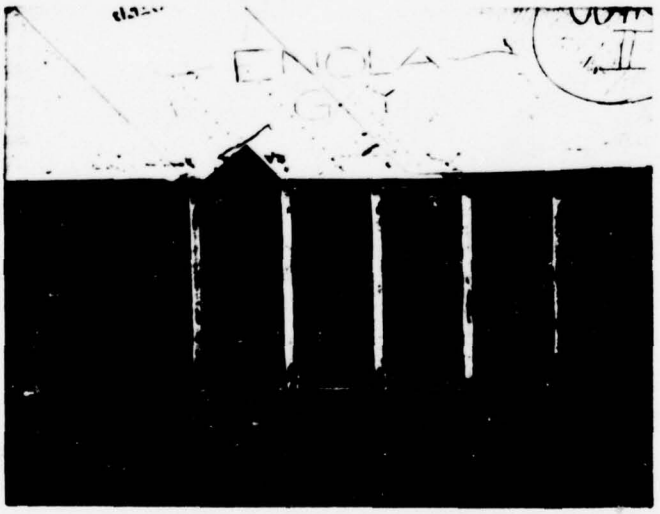

b) Side View

FIGURE III-3. CLAMPING FRAME

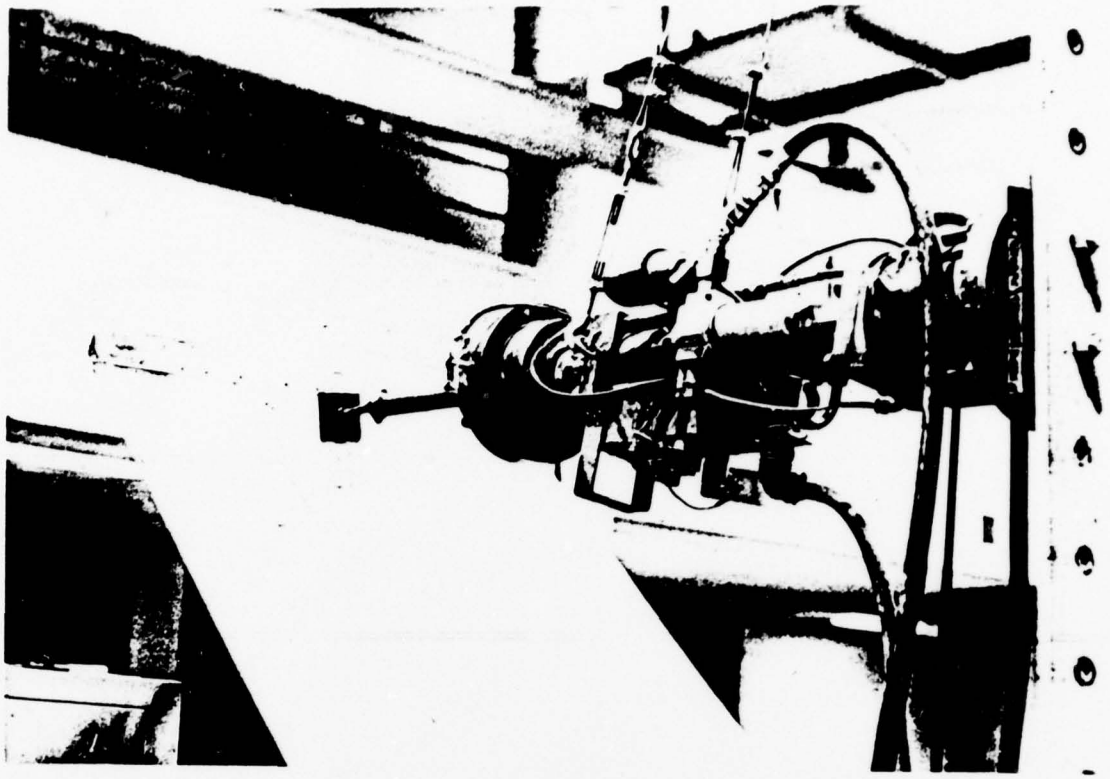

a) Hydraulic Actuator

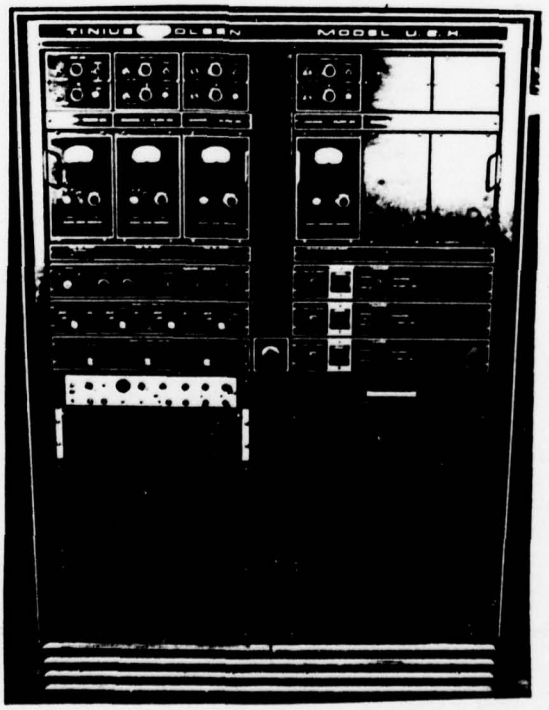

b) Control Panel

FIGURE III-4. STATIC DEFLECTION LOADING APPARATUS

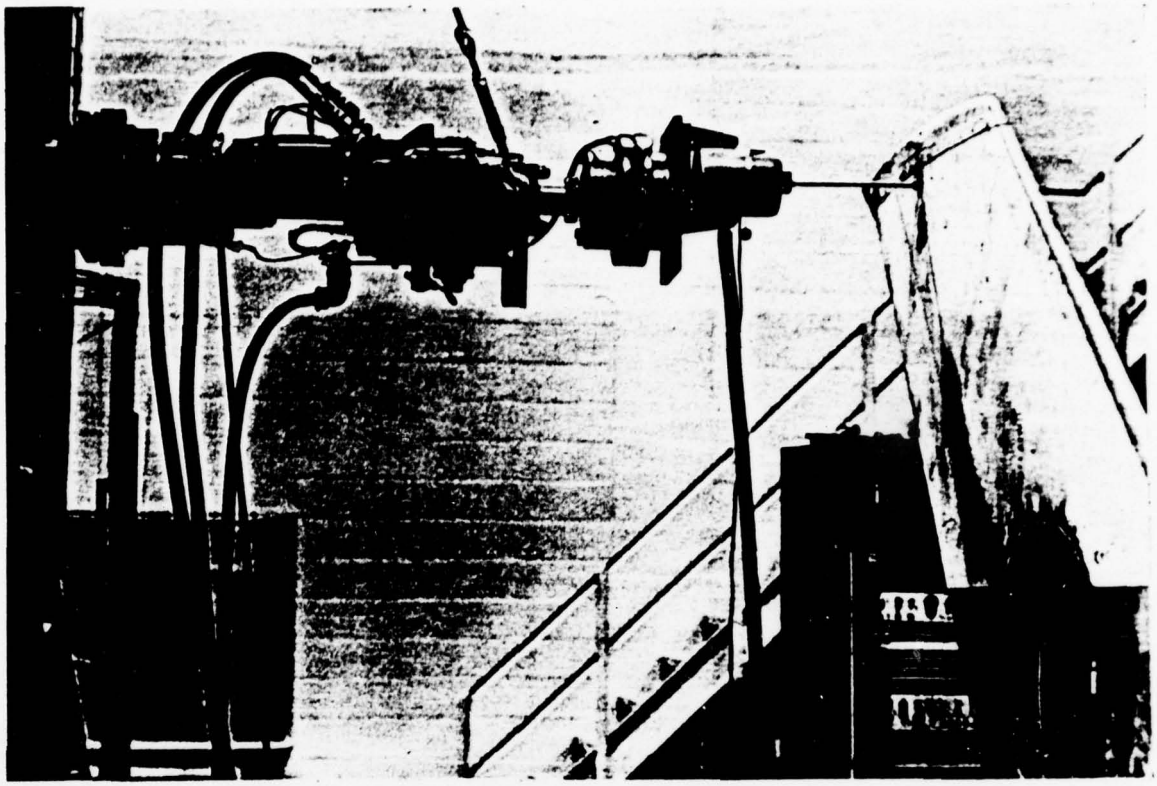

a) Electronic Shaker

b) Pluck Test

FIGURE III-5. DYNAMIC LOADING METHODS

Instrumentation used during the experimental program included accelerometers, velocity transducers and displacement transducers which were checked and monitored by an oscilloscope and recorded on a Brush strip chart recorder, portions of which are shown in Figure III-6. Data were then digitized with a Tektronix digitizing table and then interpreted and studied in detail with the Tektronix intelligent graphic system.

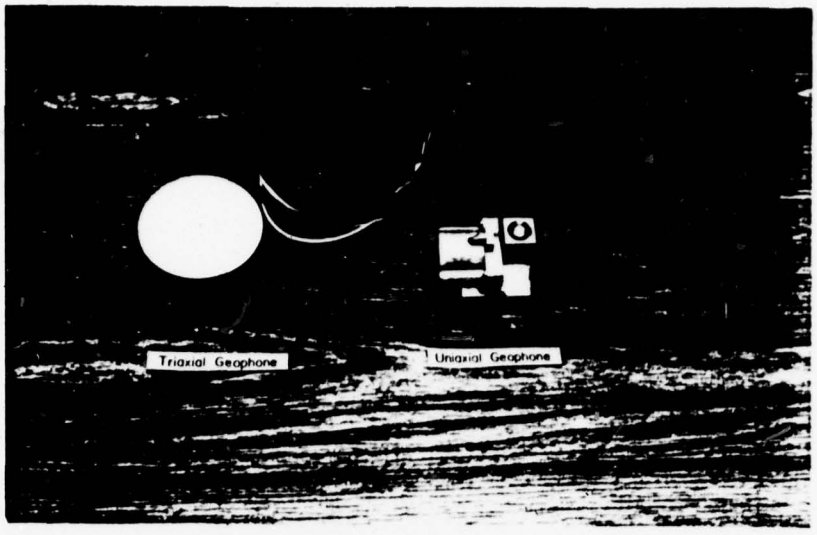

a) Velocity Transducers

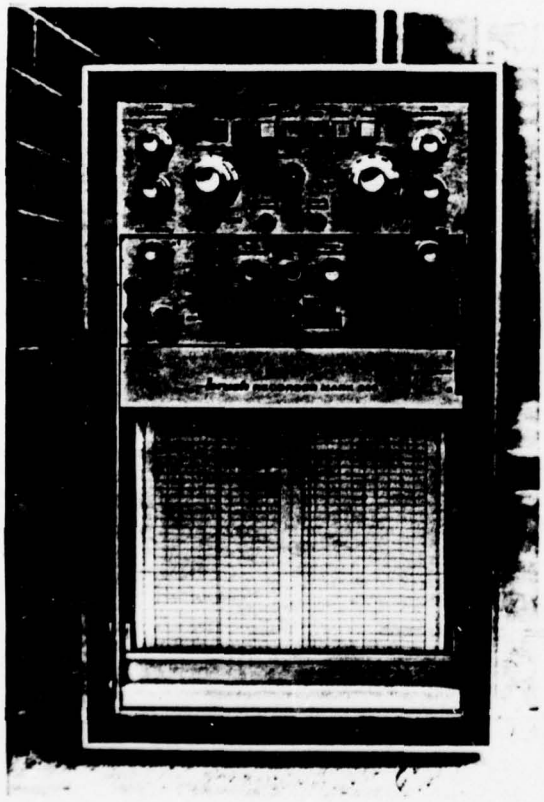

b) Strip Chart Recorder

c) Oscilliscope

FIGURE III-6. INSTRUMENTATION

IV. RESULTS

A. Experimental

Three independent laboratory tests were performed on the damaged and undamaged stabilators: static deflection tests, pluck tests, and forced vibration tests. Four different stabilators were tested with circular damage centered at four different locations (Ref. Fig. IV-1). Results are reported herein for damage diameters equal to 0, 12, 18, and 24 inches.

It was observed during the conduct of this research that comparisons of the undamaged responses of the first three stabilators were reasonably consistent. However, the fourth stabilator tested appeared to be considerably more flexible than the first three. Upon close examination of the fourth stabilator, it was found that several rivets in the trailing edge were loose. It was further observed that the section of the stabilator root available for clamping into the support was less than with the other three stabilators. These factors in combination with inherent variabilities in the stabilator construction apparently resulted in a more flexible stabilator response.

1. Static Tests

A static test consisted of mounting a particular stabilator vertically and subjecting it to a point load at the tip of the stabilator (Ref. Fig. IV-2). Static deflections were then taken at eight separate locations on the stabilator surface as shown in Figure IV-3. The point load was applied in increments of 50 lb until the deflection at the tip reached approximately 0.5 inch.

The raw data taken from the static tests on the four different stabilators are presented in Tables IV-1, IV-2, IV-3, and IV-4. The

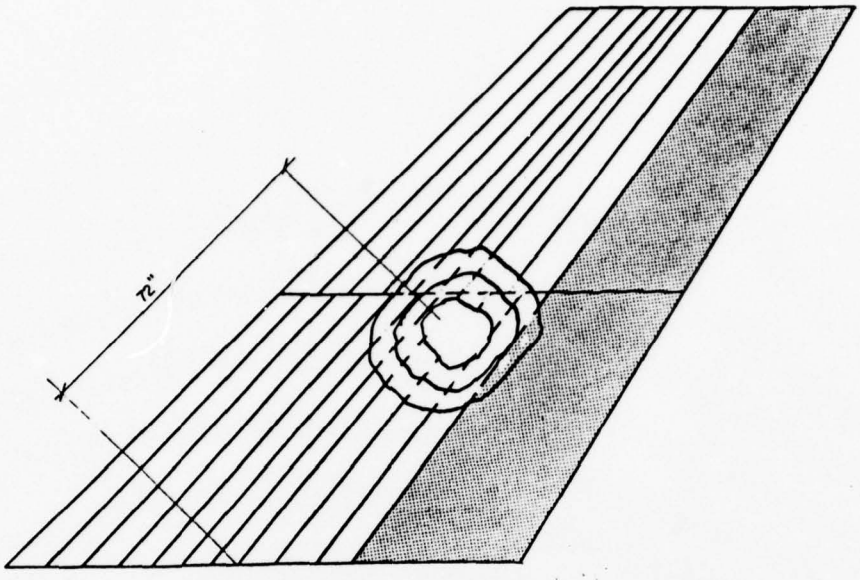

a) Stabilator I

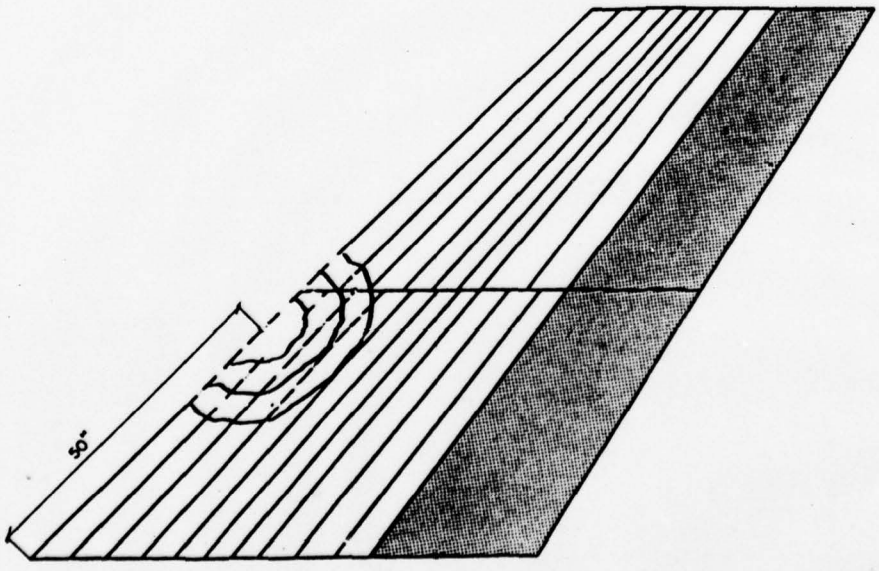

b) Stabilator II

FIGURE IV-1. DAMAGED F3H STABILATORS

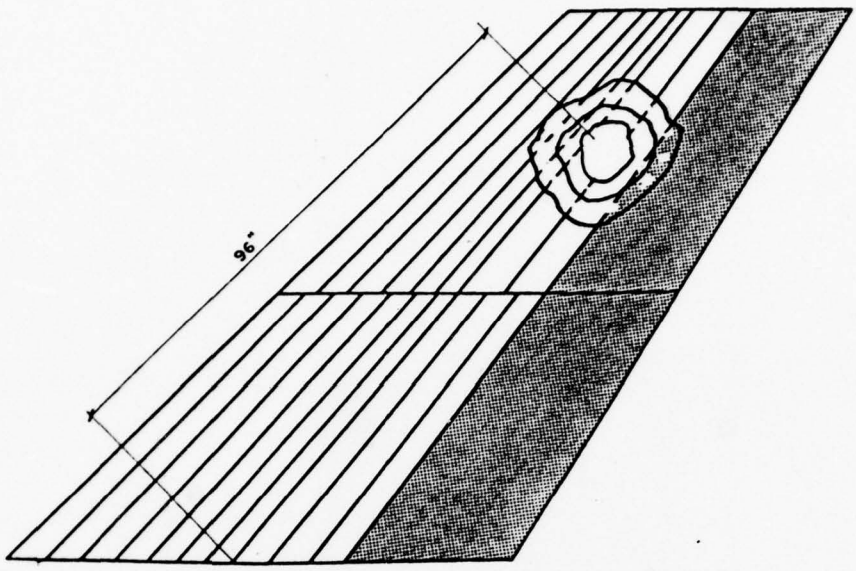

c) Stabilator III

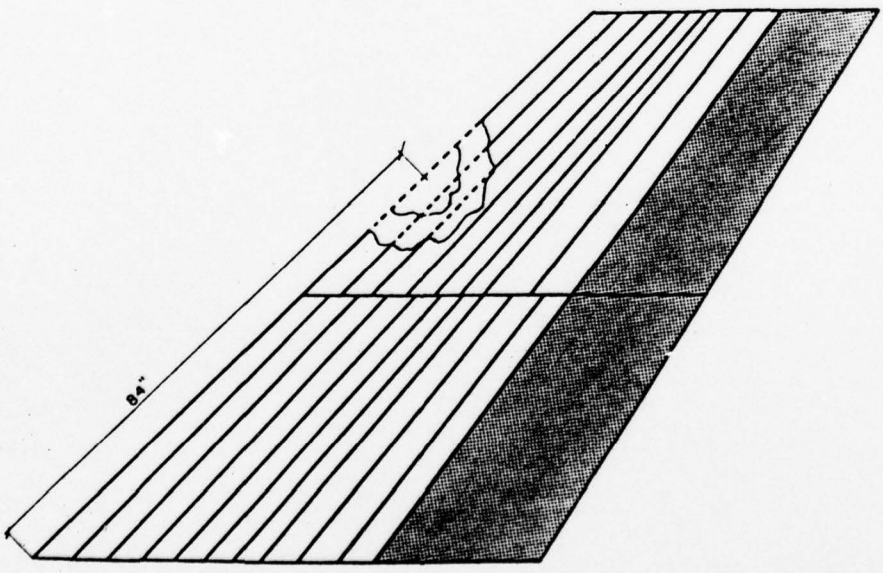

d) Stabilator IV

FIGURE IV-1. DAMAGED F3H STABILATORS (Cont'd.)

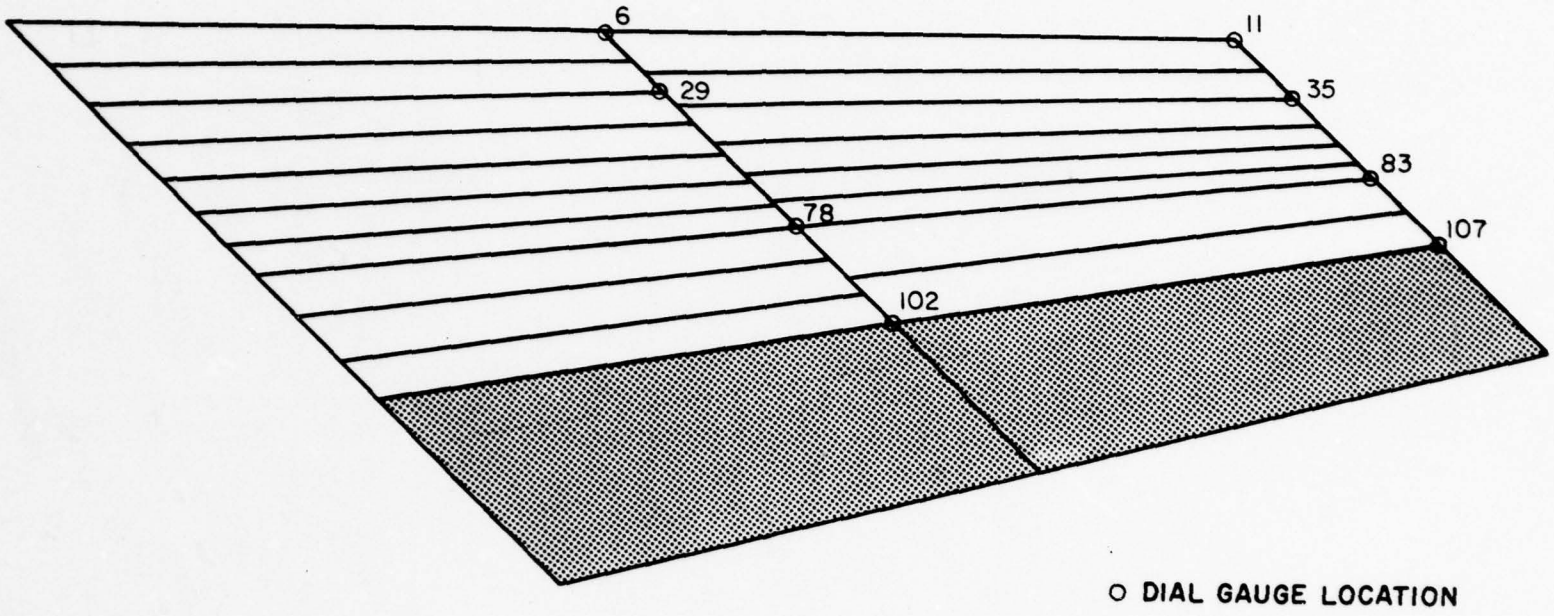

FIGURE IV-2. DIAL GAUGE LOCATIONS FOR STATIC TESTS

TABLE IV-1. WING I STATIC DATA

(a) Wing I Node 6
Static Deflections (inches)

Damage Diameter →		0"	12"	18"	24"
Load lbs	0	0	0	0	0
↓	50	0.013	0.003	0.017	0.020
	100	0.028	0.012	0.035	0.047
	150	0.043	0.032	0.054	
	200	0.059		0.071	
	250	0.075			

(b) Wing I Node 11
Static Deflections (inches)

Damage Diameter →		0"	12"	18"	24"
Load lbs	0	0	0	0	0
↓	50	0.057	0.078	0.060	0.142
	100	0.113	0.157	0.162	0.277
	150	0.174	0.241	0.277	
	200	0.235		0.367	
	250	0.300			

(c) Wing I Node 29
Static Deflections (inches)

Damage Diameter →		0"	12"	18"	24"
Load lbs	0	0	0	0	0
↓	50	0.015	0.018	0.024	0.036
	100	0.034	0.036	0.048	0.074
	150	0.051	0.055	0.072	
	200	0.070		0.094	
	250	0.089			

(d) Wing I Node 35
Static Deflections (inches)

Damage Diameter →		0"	12"	18"	24"
Load lbs	0	0	0	0	0
↓	50	0.063	0.083	0.095	0.174
	100	0.122	0.161	0.205	0.174
	150	0.188	0.252	0.325	
	200	0.254		0.425	
	250	0.324			

TABLE IV-1. WING I STATIC DATA (cont'd.)

(e) Wing I Node 78
Static Data

Damage Diameter →		0"	12"	18"	24"
Load lbs	0	0	0	D	D
↓	50	0.019	0.024	A	A
	100	0.042	0.049	M	M
	150	0.065	0.076	A	A
	200	0.088		G	G
	250	0.113		E	E

(f) Wing I Node 83
Static Data

Damage Diameter →		0"	12"	18"	24"
Load lbs	0	0	0	0	0
↓	50	0.072	0.097	0.100	0.194
	100	0.135	0.193	0.223	0.342
	150	0.207	0.296	0.361	
	200	0.280		0.474	
	250	0.358			

(g) Wing I Node 102
Static Data

Damage Diameter →		0"	12"	18"	20"
Load lbs	0	0	0	0	0
↓	50	0.023	0.024	0.042	0.067
	100	0.052	0.057	0.084	0.133
	150	0.079	0.093	0.128	
	200	0.109		0.167	
	250	0.139			

(h) Wing I Node 107
Static Data

Damage Diameter →		0"	12"	18"	20"
Load lbs	0	0	0	0	0
↓	50	0.078	0.101	0.096	0.214
	100	0.144	0.202	0.227	0.365
	150	0.222	0.310	0.382	
	200	0.301		0.501	

TABLE IV-2. WING II STATIC DATA

(a) Wing II Node 6
Static Deflections (inches)

Damage Diameter →	0"	12"	18"	24"
Load lbs 0	0	0	0	0
↓ 50	0.012	0.011	0.013	0.013
100	0.025	0.024	0.024	0.024
150	0.037	0.036	0.036	
200	0.050		0.049	
250	0.063		0.061	

(b) Wing II Node 11
Static Deflecions (inches)

Damage Diameter →	0"	12"	18"	24"
Load lbs 0	0	0	0	0
↓ 50	0.049	0.060	0.061	0.113
100	0.104	0.124	0.138	0.233
150	0.159	0.190	0.212	
200	0.219		0.285	
250	0.272		0.358	

(c) Wing II Node 29
Static Deflections (inches)

Damage Diameter →	0"	12"	18"	24"
Load lbs 0	0	0	0	0
↓ 50	0.014	0.013	0.015	0.014
100	0.029	0.028	0.028	0.027
150	0.043	0.042	0.043	
200	0.058		0.058	
250	0.073		0.072	

(d) Wing II Node 35
Static Deflections (inches)

Damage Diameter →	0"	12"	18"	24"
Load lbs 0	0	0	0	0
↓ 50	0.053	0.063	0.072	0.130
100	0.114	0.130	0.152	0.268
150	0.172	0.198	0.234	
200	0.232		0.314	

TABLE IV-2. WING II STATIC DATA (Cont'd.)

(e) Wing II Node 78
Static Deflections (inches)

Damage Diameter →		0"	12"	18"	24"
Load lbs	0	0	0	0	0
↓	50	0.020	0.018	0.019	0.019
	100	0.040	0.038	0.038	0.038
	150	0.060	0.058	0.057	
	200	0.081		0.078	
	250	0.101		0.096	

(f) Wing II Node 83
Static Deflections (inches)

Damage Diameter →		0"	12"	18"	24"
Load lbs	0	0	0	0	0
↓	50	0.061	0.074	0.077	0.165
	100	0.130	0.150	0.171	0.348
	150	0.197	0.226	0.268	
	200	0.265		0.362	
	250	0.337		0.456	

(g) Wing II Node 102
Static Deflections (inches)

Damage Diameter →		0"	12"	18"	24"
Load lbs	0	0	0	0	0
↓	50	0.024	0.025	0.024	0.023
	100	0.049	0.050	0.047	0.046
	150	0.073	0.075	0.072	
	200	0.099		0.097	
	250	0.124		0.120	

(h) Wing II Node 107
Static Deflections (inches)

Damage Diameter →		0"	12"	18"	24"
Load lbs	0	0	0	0	0
↓	50	0.065	0.074	0.089	0.192
	100	0.137	0.161	0.193	0.391
	150	0.209	0.243	0.300	
	200	0.280		0.402	
	250	0.357		0.507	

TABLE IV-3. WING III STATIC DATA

(a) Wing III Node 6
Static Deflections (inches)

Damage Diameter →		0"	12"	18"	24"
Load lbs	0	0	0	0	D
	50	0.014	0.013	0.009	A
	100	0.027	0.026	0.021	M
	150	0.042	0.039	0.035	A
	200	0.057	0.053	0.046	G
	250	0.072	0.066	0.059	E

(b) Wing III Node 11
Static Deflections (inches)

Damage Diameter →		0"	12"	18"	24"
Load lbs	0	0	0	0	0
	50	0.058	0.052	0.034	0.011
	100	0.115	0.110	0.090	0.104
	150	0.178	0.171	0.151	0.159
	200	0.247	0.238	0.215	0.219
	250	0.318		0.288	0.284

(c) Wing III Node 29
Static Deflections (inches)

Damage Diameter →		0"	12"	18"	24"
Load lbs	0	0	0	0	0
	50	0.016	0.015	0.010	0.004
	100	0.032	0.031	0.025	0.019
	150	0.049	0.048	0.041	0.035
	200	0.066	0.064	0.058	0.051
	250	0.084	0.082	0.074	0.068

(d) Wing III Node 35
Static Deflections (inches)

Damage Diameter →		0"	12"	18"	24"
Load lbs	0	0	0	0	0
	50	0.062	0.054	0.039	0.045
	100	0.124	0.117	0.100	0.115
	150	0.189	0.180	0.166	0.175
	200	0.263	0.250	0.231	0.241
	250	0.338		0.314	0.313

TABLE IV-3. WING III STATIC DATA (Cont'd.)

(e) Wing III Node 78
Static Deflections (inches)

Damage Diameter →		0"	12"	18"	24"
Load lbs	0	0	0	0	0
↓	50	0.022	0.022	0.018	0.013
	100	0.044	0.045	0.040	0.037
	150	0.067	0.069	0.065	0.062
	200	0.092	0.095	0.090	0.089
	250	0.117	0.120	0.111	0.112

(f) Wing III Node 83
Static Deflections (inches)

Damage Diameter →		0"	12"	18"	24"
Load lbs	0	0	0	0	0
↓	50	0.069	0.059	0.041	0.050
	100	0.137	0.130	0.108	0.128
	150	0.208	0.200	0.183	0.195
	200	0.289	0.278	0.259	0.272
	250	0.371		0.345	0.353

(g) Wing III Node 102
Static Deflections (inches)

Damage Diameter →		0"	12"	18"	24"
Load lbs	0	0	0	0	0
↓	50	0.027	0.028	0.014	0.013
	100	0.054	0.056	0.040	0.042
	150	0.033	0.086	0.070	0.072
	200	0.112	0.117	0.101	0.104
	250	0.143	0.148	0.133	0.138

(h) Wing III Node 107
Static Deflections (inches)

Damage Diameter →		0"	12"	18"	24"
Load lbs	0	0	0	0	0
↓	50	0.0175	0.062	0.047	0.060
	100	0.148	0.138	0.120	0.132
	150	0.224	0.212	0.197	0.209
	200	0.310	0.296	0.280	0.293
	250	0.397		0.371	0.380

TABLE IV-4. WING IV STATIC DATA

(a) Wing IV Node 6
Static Deflections (inches)

Damage Diameter →	0"	12"	18"	24"
Load lbs 0	0	0		
↓ 50	0.014	0.16		
100	0.032	0.034		
150	0.048	0.052		
200	0.066	0.070		
250	0.085	0.090		

(b) Wing IV Node 11
Static Deflections (inches)

Damage Diameter →	0"	12"	18"	24"
Load lbs 0	0	0	0	
↓ 50	0.068	0.077	0.063	
100	0.138	0.151	0.136	
150	0.213	0.231	0.213	
200	0.294		0.296	
250	0.378			

(c) Wing IV Node 29
Static Deflections (inches)

Damage Diameter →	0"	12"	18"	24"
Load lbs 0	0	0		
↓ 50	0.016	0.018		
100	0.037	0.040		
150	0.056	0.060		
200	0.078	0.082		
250	0.100	0.105		

(d) Wing IV Node 35
Static Deflections (inches)

Damage Diameter →	0"	12"	18"	24"
Load lbs 0	0	0	0	
↓ 50	0.071	0.082	0.070	
100	0.146	0.163	0.148	
150	0.224	0.247	0.229	
200	0.308		0.315	
250	0.395			

TABLE IV-4. WING IV STATIC DATA (Cont'd.)

(e) Wing IV Node 78
Static Deflections (inches)

Damage Diameter →	0"	12"	18"	24"
Load lbs ↓ 0	0	0		
50	0.022	0.024		
100	0.048	0.052		
150	0.076	0.081		
200	0.105	0.113		
250	0.142	0.148		

(f) Wing IV Node 83
Static Deflections (inches)

Damage Diameter →	0"	12"	18"	24"
Load lbs ↓ 0	0	0	0	
50	0.080	0.088	0.076	
100	0.162	0.178	0.162	
150	0.249	0.268	0.252	
200	0.340		0.345	
250	0.436			

(g) Wing IV Node 102
Static Deflections (inches)

Damage Diameter →	0"	12"	18"	24"
Load lbs ↓ 0	0	0		
50	0.024	0.011		
100	0.055	0.044		
150	0.088	0.080		
200	0.123	0.117		
250	0.160	0.157		

(h) Wing IV Node 107
Static Deflections (inches)

Damage Diameter →	0"	12"	18"	24"
Load lbs ↓ 0	0	0	0	
50	0.069	0.085	0.078	
100	0.159	0.183	0.170	
150	0.252	0.277	0.267	
200	0.352		0.366	
250	0.453			

missing deflection values in the tables are the result of the induced damage removing the stabilator material in the measurement area. It should be noted that during the first loading increment some instrument error was incurred. This problem is consistent with the use of mechanical dial gauges. The stabilator stiffnesses used in subsequent calculations were determined by ignoring the first load in increment.

The experimental facility in which the stabilators were mounted ideally should have completely limited the rotation at the point of support. However, as a matter of practicality the ideal situation was not achieved and significant rotation was observed at the root of the stabilator. In order to determine the effect of the support rotation on the observed stabilator deflections, deflections were measured along the main stabilator spar at various increments from the stabilator support. Figure IV-3 presents the stabilator deflection at eight different points along the main spar of stabilator IV as a function of the distance from the support. An interpolation function was passed through the points so that continuous deflection function could be plotted. Then a tangent was drawn to the deflection function at the point of support to evaluate the relative effect of support rotation as a function of distance from the support.

The experimental static deflection data reported herein was not modified to account for the support rotation because the primary objective of the experiment phase was to observe response variation trends as a function of damage magnitude. It was the opinion of the writers that the presence of the linear hinge would have little effect on stiffness variation.

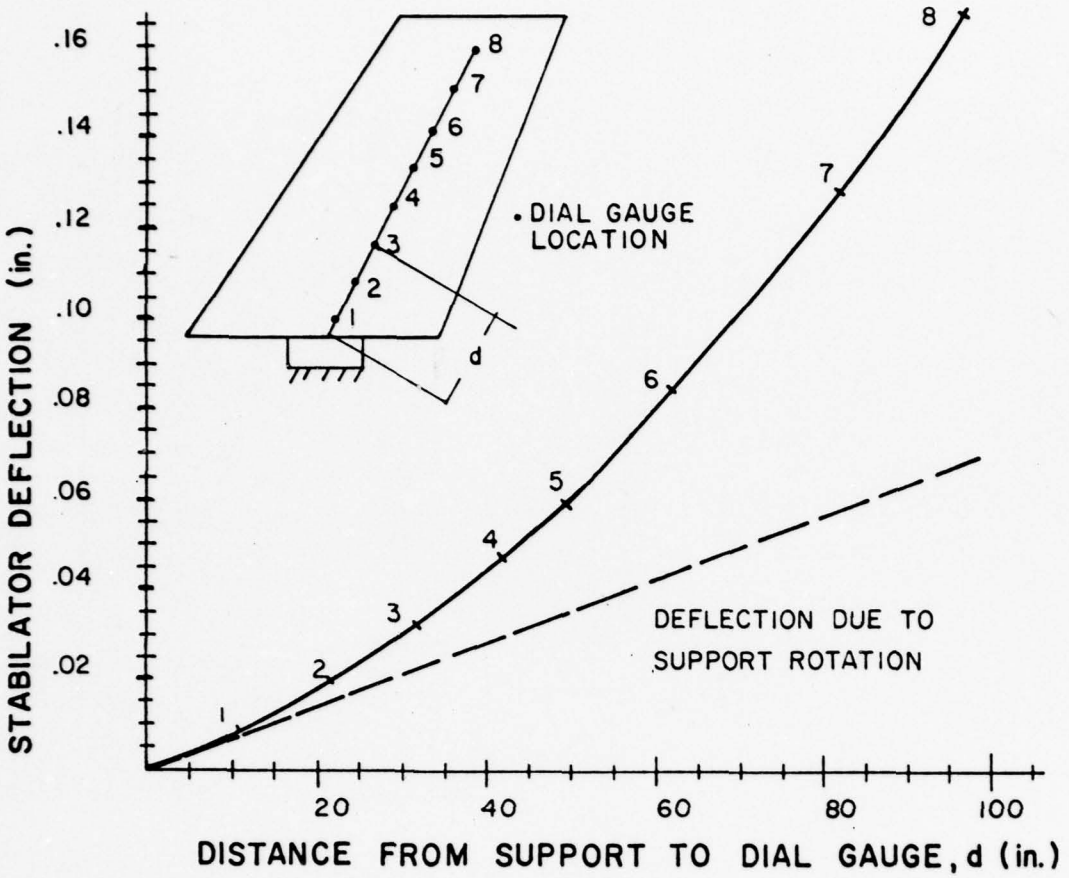

FIGURE IV-3. DEFLECTION RESULTING FROM SUPPORT ROTATION

2. Pluck Tests

A pluck test consisted of placing a preload on the stabilator and then removing the load instantaneously and allowing the stabilator to experience a free oscillation. Both geophones and accelerometers were mounted on the stabilator and their continuous output was recorded on a brush recorder. The primary objectives of the pluck tests were to determine the variation of the fundamental frequency of the stabilator with damage variation and to determine an estimate of the damping present in the stabilator.

Table IV-5 presents the measured fundamental frequencies of the F3H stabilators tested for four levels of damage. It should be remembered that the presence of the observed support rotation reduced the stabilator stiffness resulting in a fundamental frequency reduction. However, the variations of the fundamental frequency with damage level should be relatively unaffected since the characteristics of the support rotation were unaffected by the damage level.

To estimate the percentage of critical damping associated with the first fundamental frequency of the stabilator, the following equation was fit to the peaks of several cycles of the decaying stabilator velocity at different locations on the stabilator surface.

$$V_p = V_o \exp(-\beta t) \tag{4.1}$$

In the above equation, V_p is the peak velocity associated with successive velocity cycles, V_o is a constant depending upon the magnitude of the measured velocities, β is a measure of the amount of damping present, and t is the time variable (Ref. Fig. IV-4). If the logarithm of both sides of Equation (4.1) is taken, the following linear equation results:

TABLE IV-5. FUNDAMENTAL FREQUENCY (Hz) FROM PLUCK TESTS

Damage Diameter →	0"	12"	18"	24"
Wing I	16.8	15.5	13.3	10.4
Wing II	17.6	17.5	16.6	13.8
Wing III	17.0	16.8	16.7	16.6
Wing IV	16.2	15.9		

TABLE IV-6. PERCENT CRITICAL DAMPING

Damage Diameter →	0"	12"	18"	24"
Wing I	0.39	0.42	0.31	0.79
Wing II	0.20	0.20	0.40	0.27
Wing III	0.29	0.30	0.35	0.30
Wing IV	0.28	0.44		

TABLE IV-7. FUNDAMENTAL FREQUENCIES (hz) FROM FORCED VIBRATION TESTS

Damage Diameter →	0"	12"	18"	24"
Wing I	16.4	15.4	14.0	13.4
Wing II	19.8	18.1	16.8	14.6
Wing III	18.0	18.5	16.25	13.0
Wing IV	16.6	16.8	16.9	

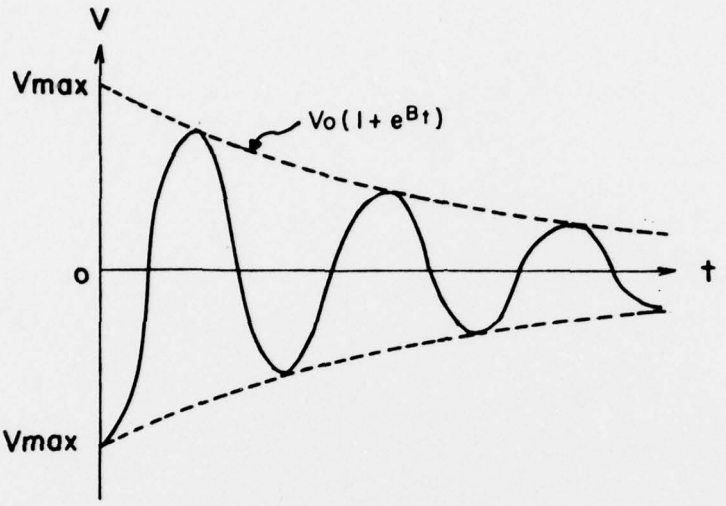

FIGURE IV-4. IDEALIZED VELOCITY DECAY FOR PLUCK TEST

$$\log(V_p) = \log(V_o) - \beta t \tag{4.2}$$

The curve fit was then accomplished using linear regression (Ref. 8). If the percentage of critical damping, C_r , by the stabilator is small it can be closely approximated by dividing the constant β by the measured fundamental circular frequency, ω_o, (radians per second).

$$C_r = \beta/\omega_o \tag{4.3}$$

Figure IV-5 presents a typical velocity decay measured on stabilator subjected to a pluck test. Similar information was recorded for each stabilator tested. Values of the percentage of critical damping experienced by the different stabilators at different levels of damage are presented in Table IV-6.

3. Forced Vibration

Forced vibration tests were performed for each stabilator situation in an attempt to locate some higher frequencies. This test consisted of exposing a stabilator to a range of frequencies while monitoring the output from geophones and accelerometers. Frequencies corresponding to velocity and acceleration amplitude maximums were recorded, and Table IV-7 presents the first natural frequencies as determined for each stabilator and damage condition.

Again, it should be emphasized that the existence of the rotation at the support precludes a direct comparison of the frequencies determined experimentally and analytically. The purpose of these tests were to establish trends in the stabilator performance.

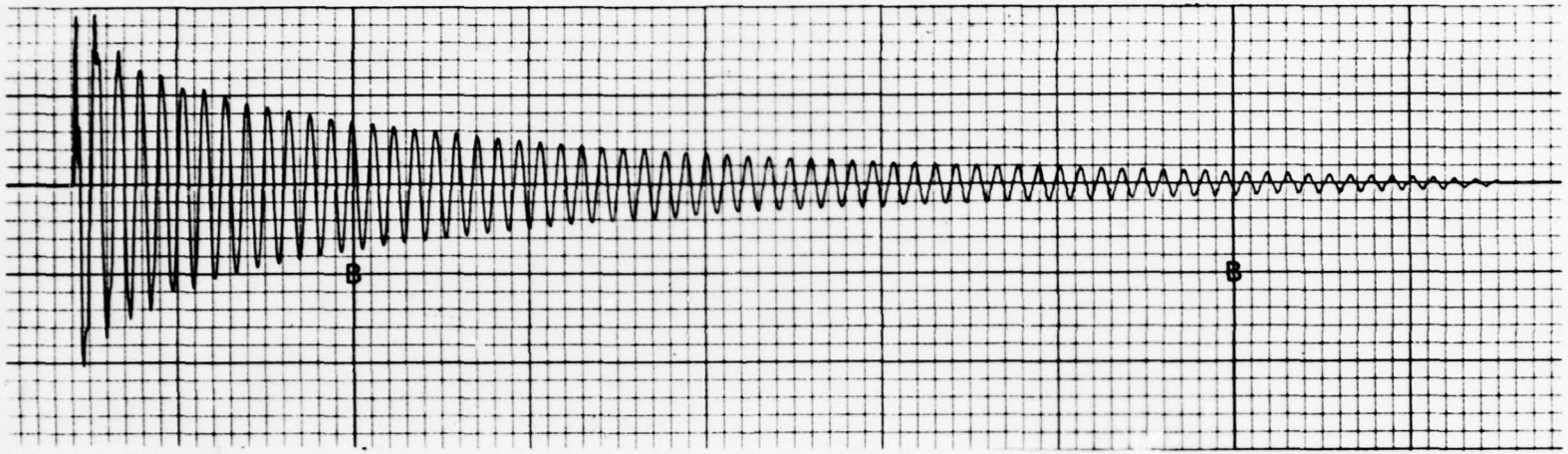

FIGURE IV-5. MEASURED VELOCITY DECAY FOR PLUCK TEST

B. Analytical Results

The analytical results reported herein are divided into four sections: verification of dynamic analysis, static deflection analysis, and analyses for damped and undamped stabilator pluck tests. Analytical results are presented for both undamaged stabilators and for stabilators with simulated 18-inch diameter damage located at the four separate locations corresponding to the experimental program. Direct comparison of the analytical results with the experimental results is impaired by the support rotation which occurred in the experimental testing program. However, after correcting for this rotation, the trends observed in the analytical results generally agree with those observed in the experimental segment of the research.

The analytically determined stabilator stiffness without support rotation is approximately 80-100 percent greater than that observed experimentally, while the analytically determined fundamental frequency is about 40-50 percent greater than the corresponding experimental values. It was demonstrated in a previous section that the added deflection resulting from the support rotation was of sufficient magnitude to cause such a difference and an examination of fundamental concepts of structural dynamics suggest that a 100 percent increase in stabilator stiffness would result in an increase in stabilator frequency of about 40 percent. Therefore, it is the opinion of the writers that the analytical solution is more representative of the true stabilator response than the experimental results.

1. Verification of Dynamic Analysis

To demonstrate the validity of the dynamic analysis presented herein a cantilever beam with distributed mass was analyzed because of its simi-

larity to the stabilator problem and the availability of exact solutions. (Ref. 8). The fundamental frequency, ω_o of the cantilever of length, l, moment of inertia, I, modulus of elasticity, F, and with mass per unit length, m, (Figure IV-6) is given by

$$\omega_o = \frac{(0.597\pi)^2}{l^2} \sqrt{\frac{EI}{m}} \qquad (4.4)$$

A test beam was chosen with a length of 100 inches, a moment of inertia of 50 $in.^4$, a modulus of elasticity of 30 x 10^6 psi, and with a mass per unit length of .04 $lb\text{-}sec^2/in$. The exact fundamental frequency of the test beam was calculated to be 68.12 rad/sec (10.84 cps). The cantilever beam was analyzed with different numbers of nodes and members and lumped masses to demonstrate the convergence characteristics of the method. The fundamental frequency was determined to be 68.5 rad/sec (10.9 cps) with the computer program with a model consisting of only two beam elements (Figure IV-6). Based on this and other comparisons not reported herein, it was concluded that the computer program is analytically correct.

2. Analytical Results for Undamped Conditions

Analytical results are reported for five different stabilator configurations: one undamaged stabilator and four stabilators with simulated 18-inch diameter damage centered around the four locations given in Figure IV-1. Each of the stabilators was mathematically subjected to three different sets of static loadings. Then given an initial deflection, each of the stabilators was instantaneously released and dynamic output concerning the undamped free vibration of the structure was generated. The three arbitrary loadings were selected in an effort to emphasize the first and

DISTRIBUTED MASS CANTILEVER BEAM

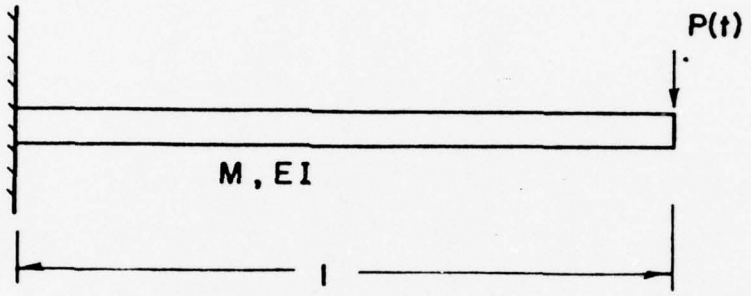

COMPUTER MODEL

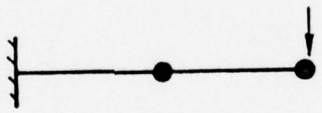

FIGURE IV-6. CANTILEVER BEAM TEST PROBLEM

second "beam" type modes and the first "torsional" type mode. However, it was subsequently determined that any one of the three loadings would result in significant modal contributions from the same set of frequencies.

Computer output for the undamaged stabilator subjected to a 350 lb static point load applied at node 83 is presented in Table IV-8. The computer results reported in Table IV-8 were taken at node points corresponding to those where similar experimental data was taken. Computer results for static cases obtained for the other two loading configurations are not presented herein, but show similar trends.

The undamped dynamic deflection output was then analyzed as described in Section II to determine the frequencies of the modal displacement amplitudes, $A_n(t)$, for the first eight most significant modal contributions. This analysis was performed using the Tektronix Intelligent Graphics System. A sample frequency analysis for a node on the undamaged stabilator is shown in Figure IV-7. The dark displacement function in Figure IV-7 represents the computer output while the lighter function was developed by considering the first eight significant modal contributions. As can be seen, the first eight modes represent nearly all of the activity at the node. Similar analyses were performed for the damaged structures and Table IV-9 presents frequencies corresponding to the first eight most significant modes for the undamaged stabilator and for the four damaged stabilators analyzed. It should be emphasized that the set of frequencies or a particular analysis includes only those frequencies causing a significant deflection contribution and not necessarily the total set of possible frequencies.

The characteristic shapes associated with the first four modal frequencies of the undamaged stabilator were determined by the methods des-

TABLE IV-8. STATIC COMPUTER-OUTPUT FOR F3H STABILATOR - NO DAMAGE

Node	Deflection
6	0.039
11	0.209
30	0.044
35	0.223
78	0.054
83	0.243
102	.063
107	0.259

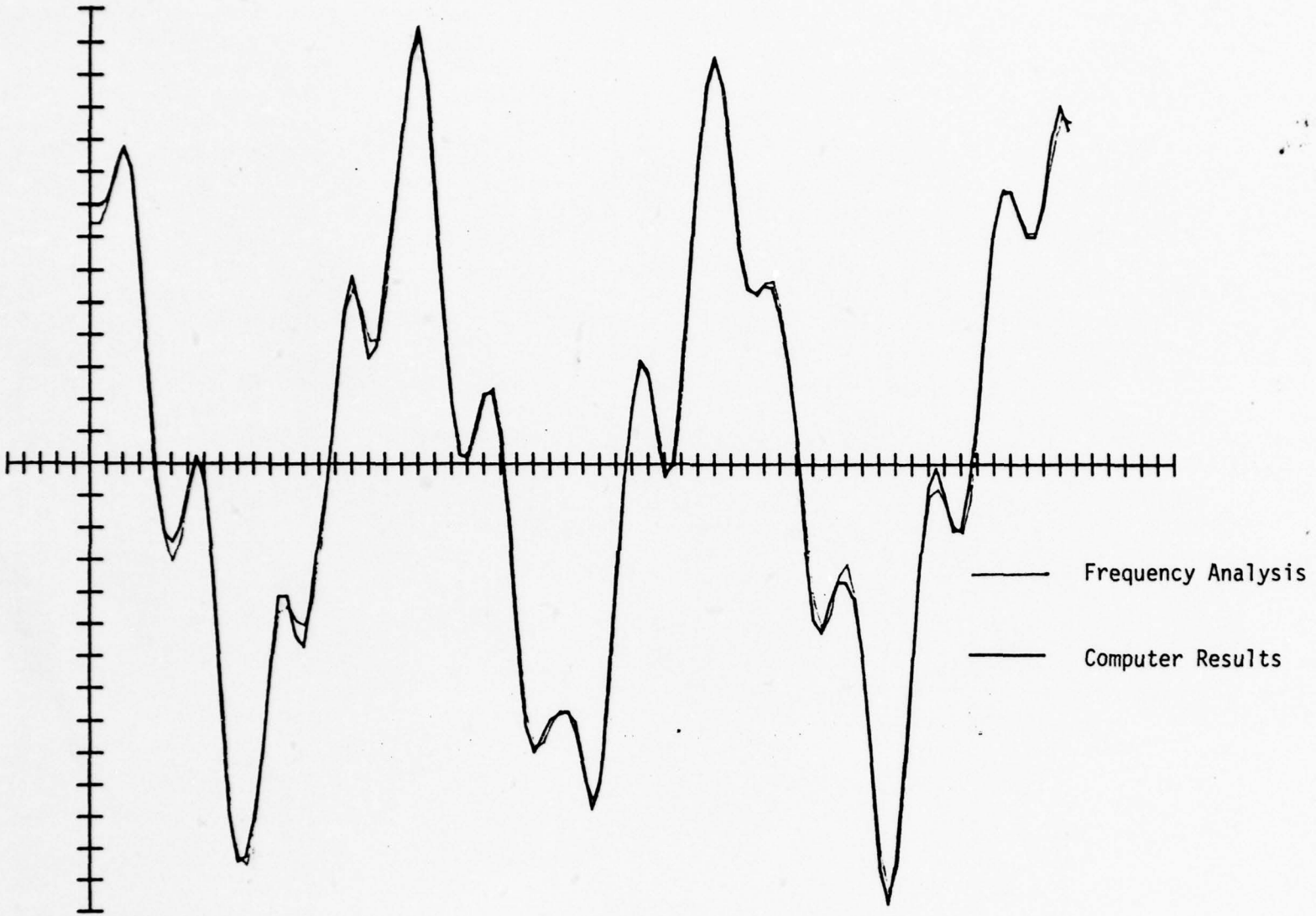

FIGURE IV-7. COMPARISON OF COMPUTER RESULTS WITH FREQUENCY ANALYSIS FOR DEFLECTION-TIME HISTORY

TABLE IV-9. PREDOMINANT FREQUENCIES FOR F3H STABILATOR FOR VARIOUS LOCATIONS OF DAMAGE (Hz)

a) Undamaged Stabilator Frequencies

26.1, 39.2, 53.9, 71.8, 78.5, 113.7, 161.9, 217.9

b)* Damaged Stabilator I (central damage location toward root)

23.5, 70.2, 109.6, 158.4, 193.4, 214.5, 251.7, 263.2

c)* Damaged Stabilator II (central damage location toward tip)

26.8, 74.5, 150.7, 214.1, 236.9, 244.5

d)* Damaged Stabilator III (leading edge damage toward root)

25.6, 70.1, 167.3, 218.4, 246.7, 255.6

e)* Damaged Stabilator IV (leading edge damage toward tip)

26.4, 80.8, 15, 217.1, 245.6, 254.6

*Damage diameter for each = 18 inches.

cribed in Section II. These characteristic shapes are presented in Figure IV-8. It can be seen by examination of these shapes that the first mode is associated with a "bending" shape while the second mode tends to be a "torsional" shape. It is difficult to make such conlusions regarding the higher modes.

3. Analytical Results for Damped Conditions

The computer analysis includes provision for damping. A constant damping coefficient, C, is employed to accomplish the damping effect in the program. The appropriate damping coefficient to be used in a particular analysis must be determined through a process of trial and error. Different values of the damping coefficient were tried in the analysis of the F3H stabilator to determine an appropriate value. Figure IV-9 presents the functional relationship between the damping coefficient, C, and the percent critical damping observed in the computer output generated for this structure. In order to achieve a percentage of critical damping comparable to that observed in the laboratory it is suggested that the value of the damping coefficient for the F3H stabilator be equal to or less than 0.00001.

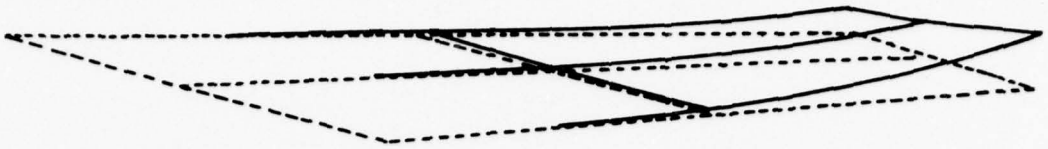

26.1 * cps

a) First Mode

* denotes frequency

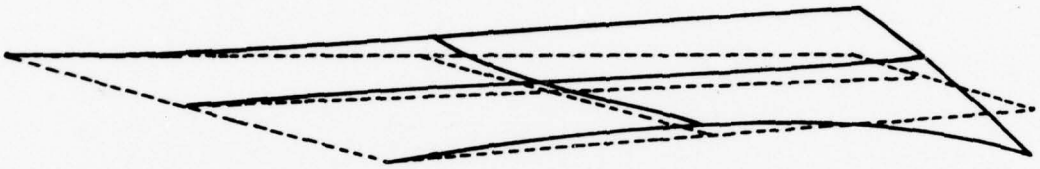

39.2 cps

b) Second Mode

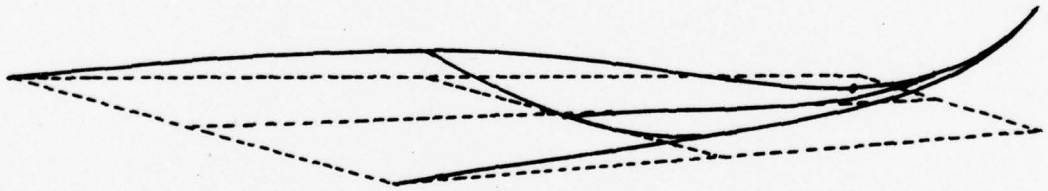

53.9 cps

c) Third Mode

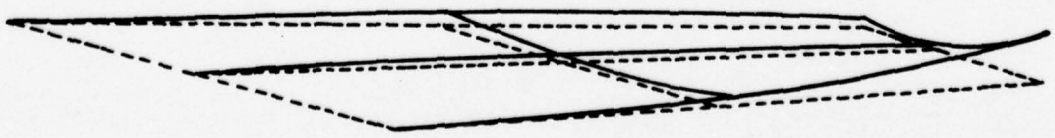

71.8 cps

d) Fourth Mode

FIGURE IV-8. F3H STABILATOR CHARACTERISTIC SHAPES

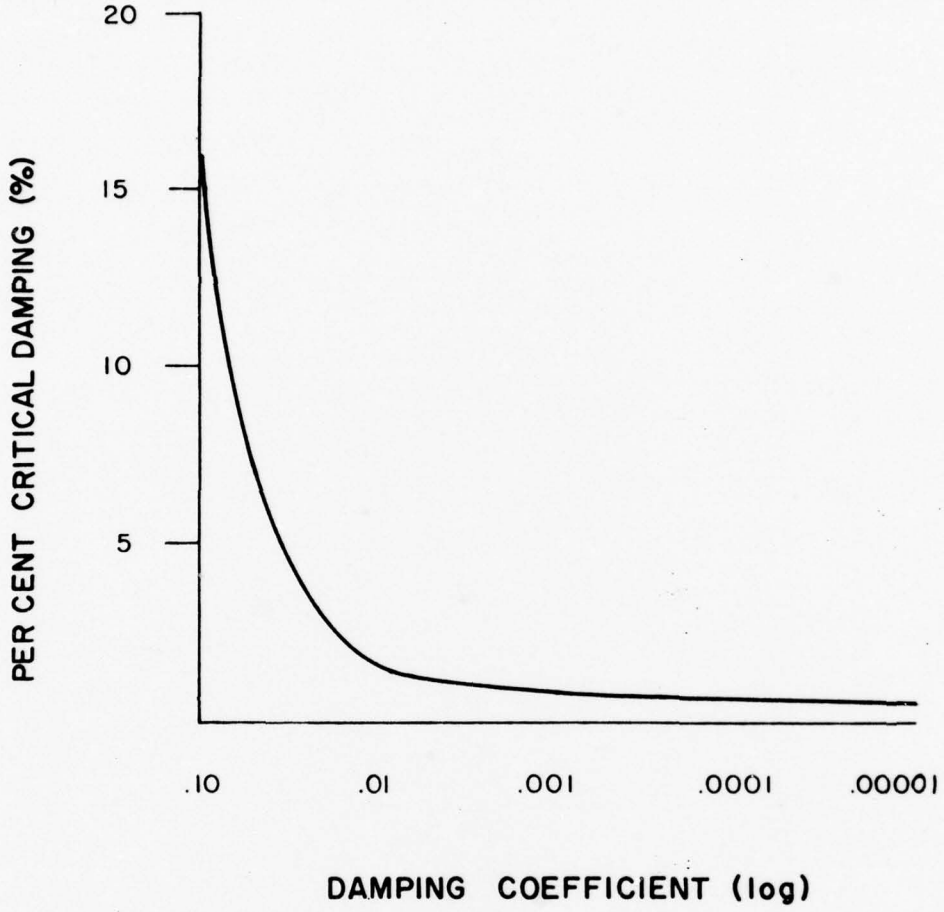

FIGURE IV-9. DAMPING RELATIONSHIPS FOR F3H STABILATOR

V. SIMPLIFIED MODEL OF STABILATOR RESPONSE

Upon reviewing the experimental data taken in the test program described previously, the following general trends became obvious: (1) the larger the level of damage for a given damage location, the greater the effect of the damage on the stiffness of the stabilator, (2) the further away from the stabilator support a given level of damage was located, the less effect it had upon the stabilator stiffness, and (3) a quadratic relationship existed between the stiffness of a stabilator and its associated fundamental frequency. These observations tend to substantiate the assumption that the stabilator system essentially behaves as though it were composed of a series of beams as was assumed in the computer model. The first two observations taken together suggest that it is valid to model the damage level for a particular situation by appropriately modifying the model member properties in the local region of damage. Further, these three observations are used as a basis to develop a simplified model of stabilator response which can be used to estimate the variation of the first fundamental frequency as a function of damage.

A. Effects of Damage Level at a Given Location

It was observed in the conduct of the first series of damaged stabilator tests that the tip stiffness of the stabilator (defined as the force required at the tip to induce a unit displacement at that point) was almost linearly related to the diameter of the induced damage for a particular damage location. Evaluation of the data taken during subsequent test series of the other three stabilators revealed that while the relationship between the stabilator tip stiffness and damage

diameter was not perfectly linear, a definite decrease in stabilator tip stiffness resulted as the damage diameter increased. A linear regression technique was employed to evaluate the "best" linear relationship between stabilator tip stiffness, K_{tip}, and damage diameter, D_{dam}, for each stabilator tested in the following form:

$$K_{tip} = a + b\, D_{dam} + \varepsilon. \qquad (5.1)$$

Where ε represents the error in the relationship and the coefficients, a and b are determined for each of the four stabilators tested. The respective values of a and b thus determined along with the corresponding correlation coefficients, r, are presented in Table V-1 for each the four stabilators tested. The discrepancy between the data taken during tests on Wing IV and that taken in previous tests are reflected in the values of the intercept coefficient, a, given in Table V-1. The linear curve-fits are presented graphically in Figure V-1.

While the relationship between the stabilator stiffness and the damage diameter is interesting, it is clear that the longitudinal stiffness of the stabilator is not uniformly distributed across the cross section of the stabilator. This is expected since the depth of the stabilator is not constant, the thickness of the skin is variable, and the thickness of the internal members change. Because of the non-uniform distribution of stiffness, the variation of tip stiffness is affected by both the location and the diameter of the damage. Therefore, the writers sought to determine a more appropriate relationship between the imposed damage and the stabilator tip stiffness.

TABLE V-1. TIP STIFFNESS-DAMAGE DIAMETER REGRESSION COEFFICIENTS

Stabilator	a	b	r
I	726	-17.4	.99
II	791	-18.1	.91
III	721	-1.13	.96
IV	588	-1.57	.79

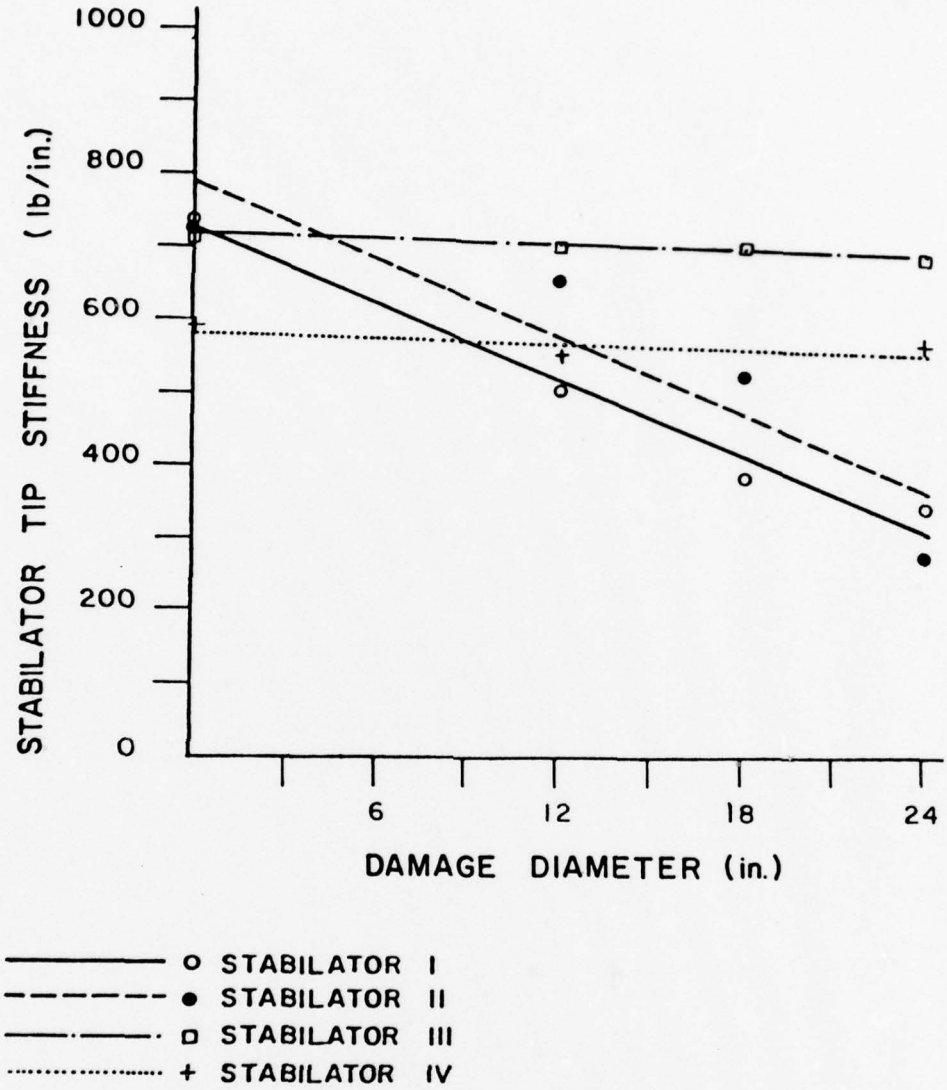

FIGURE V-1. STABILATOR TIP STIFFNESS VS. DAMAGE DIAMETER

The interior structure of the F3H stabilator consists of longitudinal channel members except the trailing edge which is composed of honeycomb construction (Figure V-2). The channel stiffeners and the honeycomb stiffener are covered with a thin metal skin which is attached with rivets and epoxy resulting in a cross-section as shown in Figure V-3. The moment of inertia, I, of the F3H cross-section can be approximated by considering only the transfer term of the parallel axis theorem. Therefore,

$$I = \int_o^W A(w)\, d(w)^2 dw \tag{5.2}$$

where A(w) is the area of the material located along the perimeter of the stabilator cross-section (largely the area of the metal skin), d(w) is the distance from the neutral axis of the cross-section to the centroid of the material concentrated along the perimeter of the stabilator cross-section, and w is the width variable of the cross-section (Ref. Fig. V-4). If it is assumed that d(w) is linearly related to the stabilator cross-section thickness, t(w), then the longitudinal moment of inertia of the stabilator cross-section should be related to the thickness of the cross-section as given by the following relationship:

$$I \propto \int_o^W A(w)\, t(w)^2\, dw. \tag{5.3}$$

If the cross-section of the stabilator is damaged (material is removed), then the moment of inertia of the cross-section removed by the damage, I_D, is assumed to be proportional to the integral in Equation (5.3) evaluated only over the area of damage yielding:

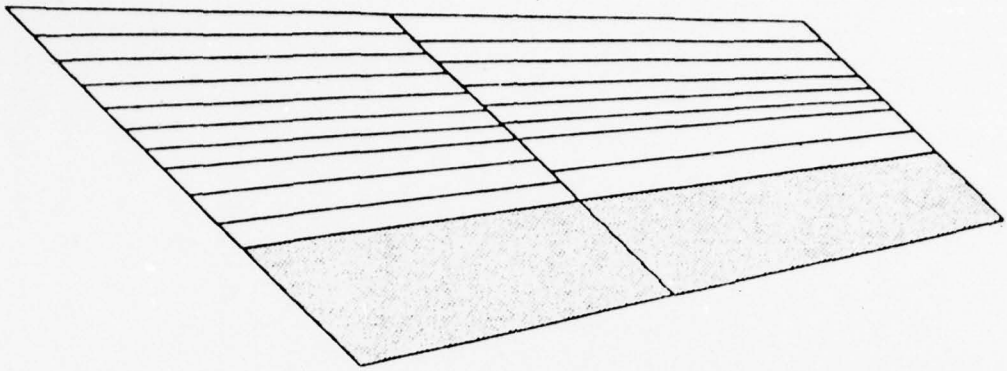

FIGURE V-2. SCHEMATIC OF STABILATOR CONSTRUCTION

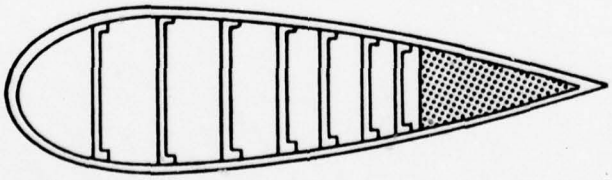

FIGURE V-3. SCHEMATIC OF STABILATOR CROSS-SECTION

$$I_D \propto \int_a^b A(w)\ t(w)^2\ dw \qquad (5.4)$$

where a and b refer to the beginning and ending of the damage area (Figure V-5). If relationship (5.4) is divided by relationship (5.3), the ratio will be approximately equal to the fraction of the original cross-sectional moment of inertia removed by the damage. This quantity is termed the transverse damage index, TDI, and is given by

$$TDI = \frac{\int_a^b A(w)\ t(w)^2\ dw}{\int_o^w A(w)\ t(w)^2\ dw} \qquad (5.5)$$

Figure V-6 presents the observed variations of the transverse damage index with variations of the stabilator tip stiffness for the four stabilators tested. In general, it can be said that as the transverse damage index increased the stabilator tip stiffness decreased. If tests had been conducted such that the only damage variable was the transverse damage index, then it would be suspected that the relationship between the stabilator tip stiffness and the transverse damage index would be approximately linear. A strictly linear relationship can be seen for a similar case of a simple cantilever beam where the stiffness of a particular section of the beam is allowed to vary.

B. Effects of Longitudinal Location of Damage

Two other factors which influenced the reduction of tip stiffness of a damaged stabilator were the longitudinal damage dimension, L_d, (damage diameter in the case of circular damage), and the longitudinal location

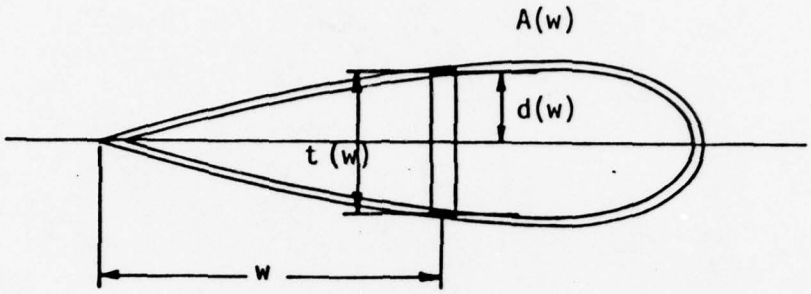

FIGURE V-4. PRESENTATION OF FACTORS INFLUENCING CROSS-SECTION STIFFENERS

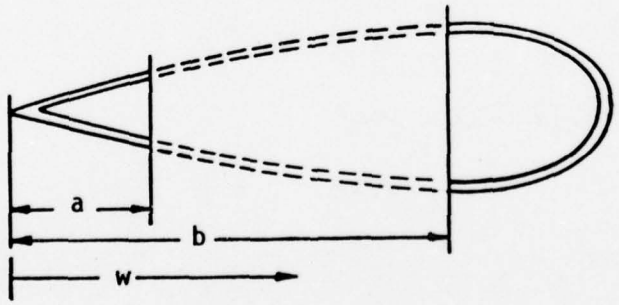

FIGURE V-5. SCHEMATIC OF DAMAGED STABILATOR CROSS-SECTION

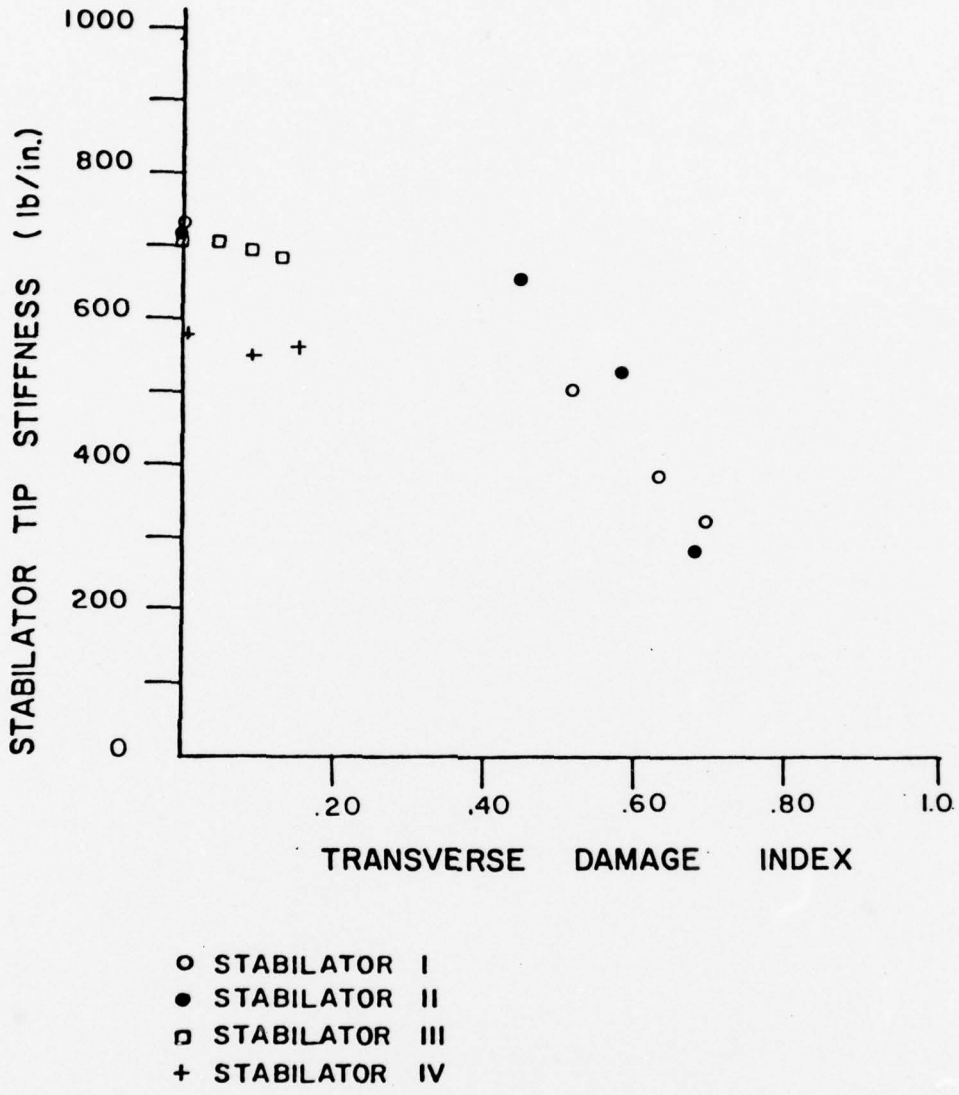

FIGURE V-6. STABILATOR TIP STIFFNESS VS. TRANSVERSE DAMAGE INDEX

of the damage center, L_c (Figure V-7). It can be shown analytically that the tip stiffness of a simple cantilever beam varies linearly with both the longitudinal damage dimension and the longitudinal center of damage. Therefore, it was assumed that a similar relationship is true for the stabilator.

It was assumed that the stabilator tip stiffness, K_{tip}, would be proportional to the longitudinal damage parameters as follows:

$$K_{tip} \alpha (L - L_d)/L \tag{5.6}$$

$$K_{tip} \alpha L_c/L \tag{5.7}$$

where L is the total longitudinal length of the stabilator along its center line (Figure V-7). Assuming that the two proportionalities represented by relationships are independent, the longitudinal damage index, LDI, is formulated in the following form

$$LDI = \frac{(L_c)\ (L-L_d)}{L^2} \tag{5.8}$$

The longitudinal damage index can vary from zero to one. When the longitudinal damage index is zero, the tip stiffness of the stabilator tends to zero as the transverse damage increases. The longitudinal damage index can go to zero if either the longitudinal damage center is at the support or if the longitudinal damage dimension is equal to the stabilator length. If the longitudinal damage center is at the tip of the stabilator and the

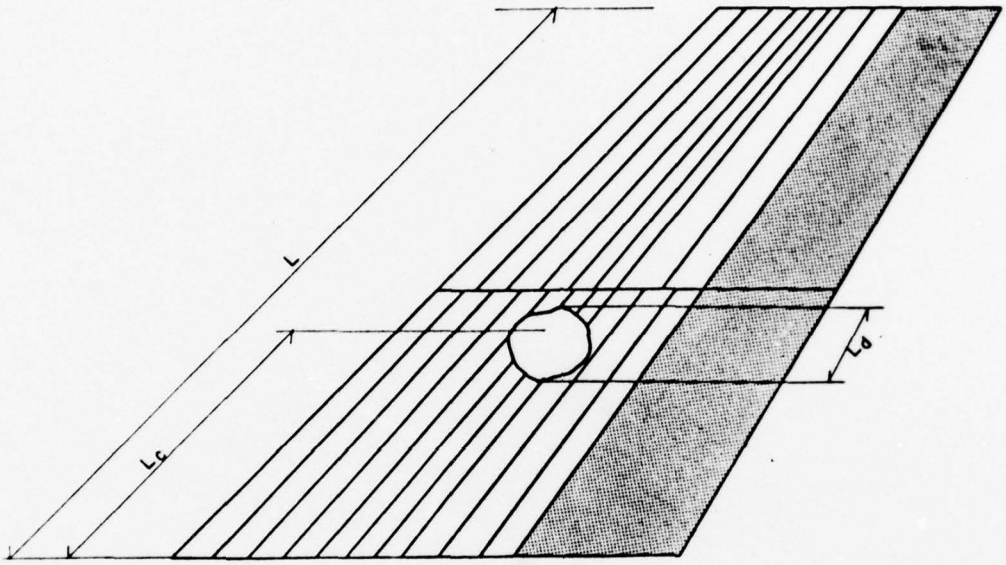

FIGURE V-7. PRESENTATION OF FACTORS INFLUENCING LONGITUDINAL DAMAGE INDEX

longitudinal damage length is zero, then the longitudinal damage index is one and hence the stabilator tip stiffness is unaffected.

Figure V-8 presents the variation of stabilator tip stiffness with changes in the longitudinal damage index. Again, tests were not conducted such that only the longitudinal damage index was permitted to vary so that firm conclusions regarding the nature of the relationship between the longitudinal damage index and the stabilator tip stiffness cannot be easily made. However, it was apparent that the stabilator tip stiffness decreased as the longtitudinal damage index decreased.

C. Relationships Between the Stabilator Tip Stiffness and the First Fundamental Frequency of the Stabilator

From elementary structural dynamics it is known that the fundamental frequency, ω_o, of a structure is proportional to the square root of the equivalent one-degree-of-freedom stiffness, K_e, divided by its equivalent one-degree-of-freedom mass, m_e, as given by

$$\omega_o \propto \sqrt{\frac{K_e}{m_e}} \tag{5.9}$$

Therefore, it would seem reasonable to assume that there would be a relationship between the equivalent one-degree-of-freedom stiffness of the stabilator and the stabilator tip stiffness. Further, it was assumed that the equivalent one-degree-of-freedom mass, m_e, remained constant so that the first fundamental frequency of the stabilator was assumed to be proportional to the square root of the stabilator tip stiffness, K_T, as given by

$$\omega_o \propto \sqrt{K_T} \tag{5.10}$$

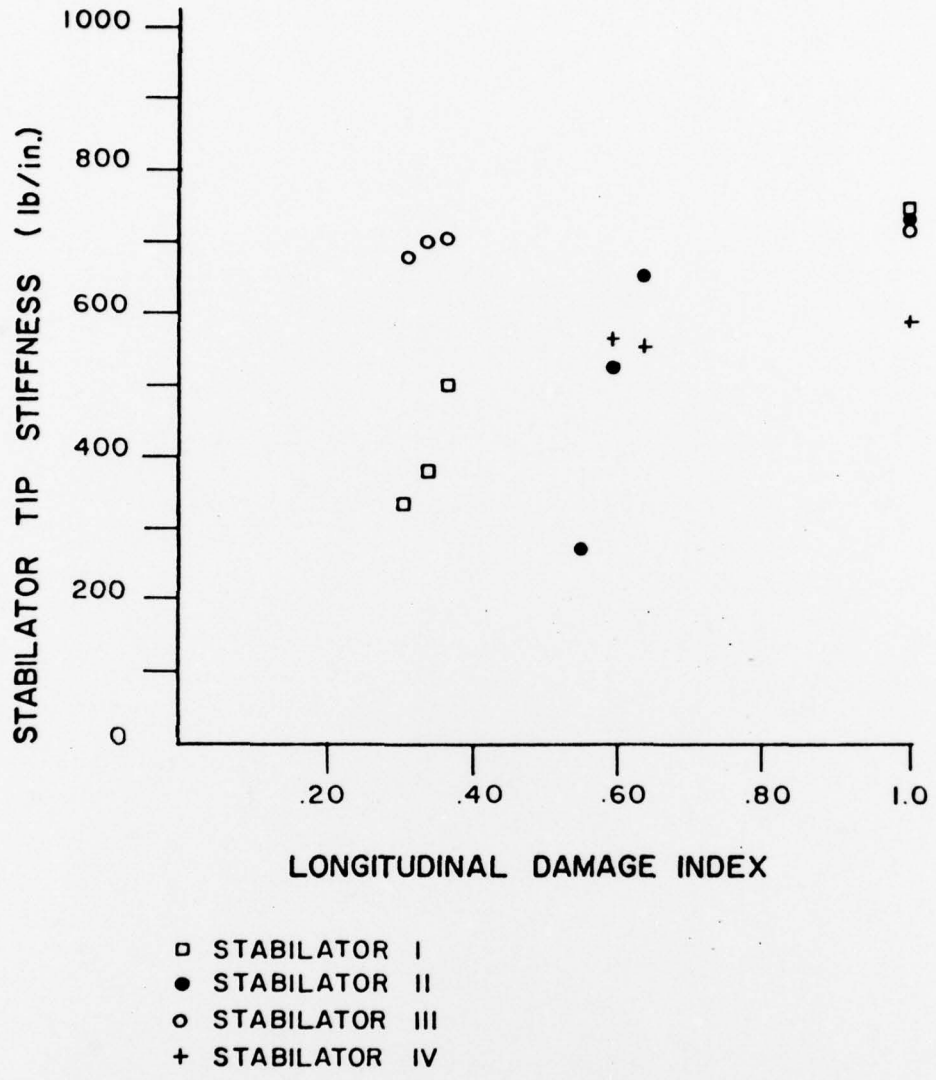

FIGURE V-8. STABILATOR TIP STIFFNESS VS. LONGITUDINAL DAMAGE INDEX

Linear regression techniques were used to find the best estimates of the coefficients, c and d, to relate the stabilator tip stiffness, K_T, and the first fundamental frequency, ω_o.

$$\omega_o = c + D(K_T)^{\frac{1}{2}} + \varepsilon \qquad (5.11)$$

Where ε represents the error involved in the curve fit. Values of the coefficients c and d and the regression coefficient, r, are presented in Table V-2. The curve-fits are presented graphically in Figure V-9 and it can be seen that the relationship between the fundamental frequencies and the stabilator tip stiffnesses for a particular damage location are strongly quadratic.

D. Simplified Response Model Formulation

The matrix structural analysis method presented herein can be used to determine changes in the dynamic characteristics of a given stabilator as a function of damage. However, the analysis requires significant data manipulation and computer time. Situations are conceivable where all that would be required is a good estimate of how much the fundamental frequency of the stabilator might change as the result of a certain level of stabilator damage. Thus, a technique was developed which would provide estimates of the variations of the fundamental frequency of a stabilator as a function of damage level and damage location. It is assumed in this estimation technique that the first fundamental frequency is a "beam" frequency, and that the variation of the equivalent one-degree-of-freedom mass of the stabilator removed during damage is negligible. The second assumption limits the usefulness of the technique to stabilators experiencing only moderate damage.

TABLE V-2. TIP STIFFNESS-FUNDAMENTAL FREQUENCY REGRESSION COEFFICIENTS

Stabilator	a	b	r
I	-0.16	0.65	.91
II	7.75	0.37	.99
III	-2.57	0.73	.96
IV	9.97	0.26	-

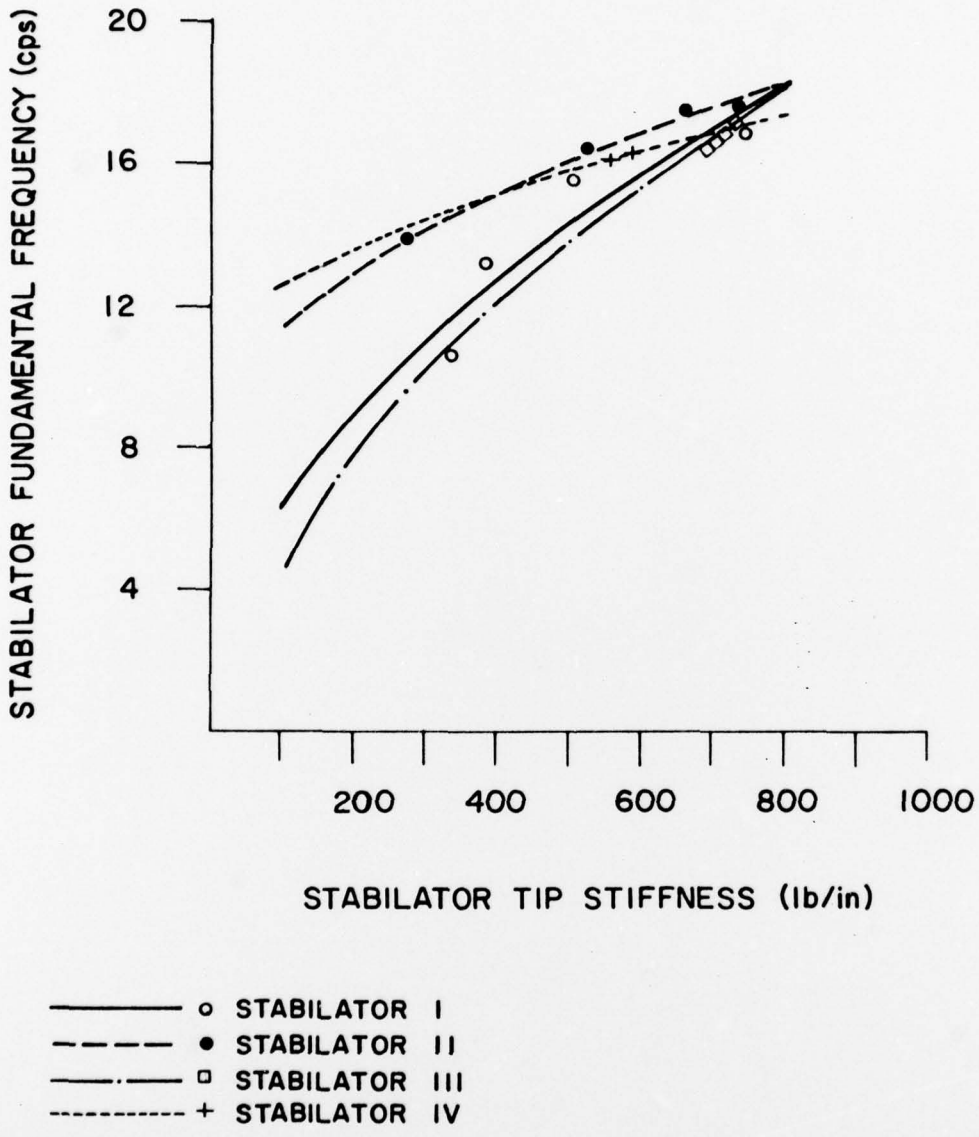

FIGURE V-9. STABILATOR FUNDAMENTAL FREQUENCY VS. STABILATOR TIP STIFFNESS

To present the stabilator response model in general terms, the fundamental frequency of a damaged stabilator was normalized by dividing by the fundamental frequency of the undamaged stabilator. Therefore, the normalized fundamental frequency of an undamaged stabilator is unity and it decreases with increasing damage.

It was assumed that the normalized equivalent one-degree-of-freedom stabilator stiffness was related to the transverse damage index and the longitudinal damage index in the following form:

$$K_e \alpha [1 + TDI (LDI - 1)]^{1/2} \qquad (5.12)$$

The relationship given in expression (5.12) is probably the most simple expression that can be used to relate the fundamental one-degree-of-freedom stiffness to the damage parameters. If the transverse damage index is zero or if the longitudinal damage index is one, then the stiffness is unity or unchanged. If the transverse damage index is one and the longitudinal damage index is zero, then the stabilator is completely severed at the root and the stiffness goes to zero. These two situations then adequately represent the extreme cases. It is possible that a more complicated expression could more closely represent the variation between the extremes, but further sophistication seems unwarranted based on the limited data base available.

The proposed relationship between the stabilator damage and its fundamental frequency is given in Figure V-10. Also, presented in this figure are the experimental observations from the four damage locations used. While the experimental data does not follow the postulated relaship exactly, it is clear that the actual damaged stabilator response is very similar to the the proposed relationship.

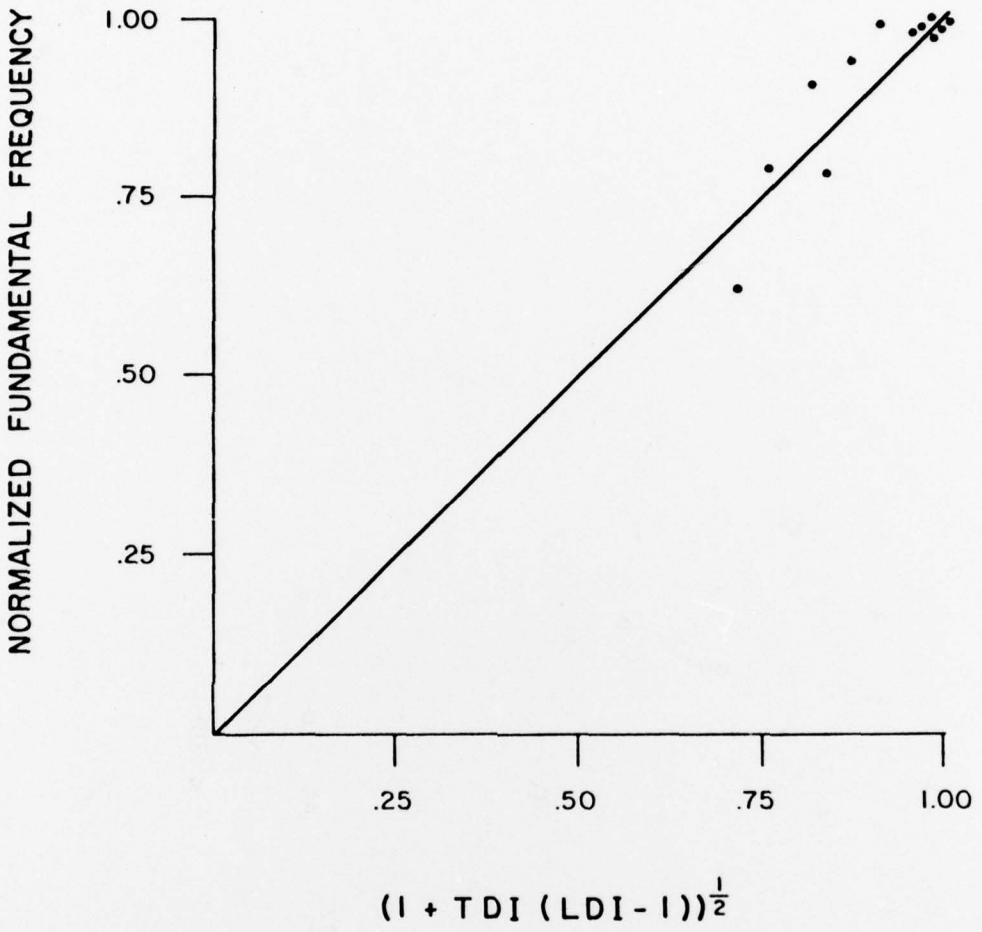

FIGURE V-10. NORMALIZED FUNDAMENTAL FREQUENCY VS. DAMAGE INDICES

To apply the stabilator response model in a less cumbersome fashion, Figure V-11 was prepared. To use this figure for a given level of damage, it is necessary to estimate the longitudinal and transverse damage indices for the particular damage level. To arrive at the values of the transverse damage index for the stabilator damages reported herein, a meticuluous procedure was employed whereby the required integrations were performed numerically. Table V-3 presents the results of the simplified model of stabilator response when applied to the stabilator test data reported herein. It should be noted that as the damage diameter increased, the percentage error incurred in the estimation process increased. This is because the equivalent mass is affected more by large amounts of damage.

To estimate the fundamental frequency change of a stabilator experiencing a certain level of damage, it is recommended that the values of the transverse damage index and the longitudinal damage index be estimated using engineering judgment. Using the method in this manner should allow the user to achieve a reasonable estimate of the fundamental frequency variation as the result of moderate amounts of damage for similar stabilator structures.

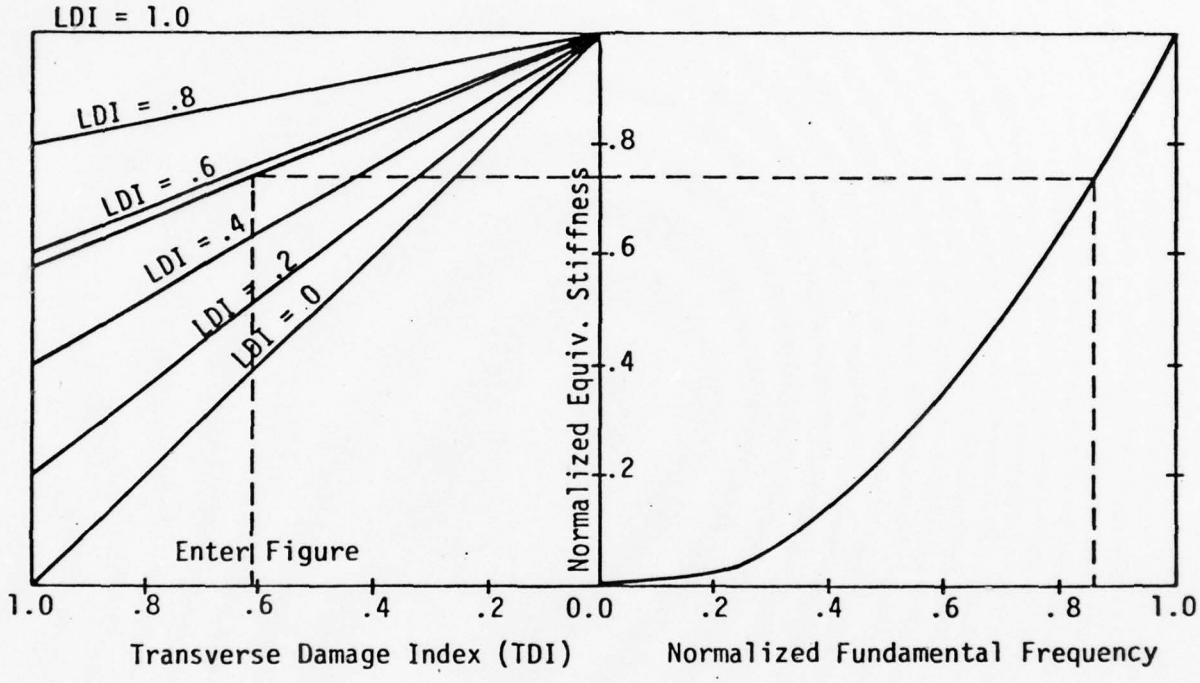

FIGURE V-11. DAMAGE/STIFFNESS/FREQUENCY RELATIONSHIPS

TABLE V-3. SIMPLIFIED STABILATOR MODE RESPONSE

Test Series	TDI	LDI	Damage Diameter (in.)	Actual Frequency (cps)	Predicted Frequency (cps)	Error (%)
I	0	1	0	16.8	16.8	-
I	.53	.37	12	15.5	15.2	2
I	.65	.34	18	13.3	14.7	11
I	.72	.32	24	10.4	14.2	37
II	0	1	0	17.6	16.8	-
II	.47	.63	12	17.5	16.8	4
II	.60	.59	18	16.6	16.4	1
II	.70	.55	24	13.8	16.0	16
III	0	1.0	0	17.0	17.0	-
III	.05	.37	12	16.8	16.8	<1
III	.09	.34	18	16.7	16.7	<1
III	.13	.32	24	16.6	16.6	<1
IV	0	1.0	0	16.2	16.2	-
IV	.09	.63	12	15.9	16.0	1

VI. SUMMARY AND CONCLUSIONS

Static and dynamic structural characteristics of a complex structure, namely a damaged aircraft stabilator, have been investigated by both experiment and analysis. A total of 60 separate laboratory tests were performed on the F3H stabilator with various damage conditions; both degree and location of damage was varied. The types of tests employed were static and dynamic with the latter comprising both pluck (suddenly released load) and forced vibration. Of primary interest was the relationships that existed between level and location of damage and structural characteristics such as stiffness, natural frequencies and damping.

Since both cost and time constraints made it impractical to conduct the number of tests that would have been necessary for accurately predicting the effects of both location and severity of damage base solely on experimental work, a mathematical model and a computer program were developed to numerically calculate the structural response for various damage conditions. The experimental results were used as the basis for several aspects of the computer program development. Although the numerical analysis made possible the study of the interactions of the various parameters, this required a relatively complicated procedure of structural modeling. Therefore, to provide a less cumbersome method to estimate the change in natural frequencies as a function of damage, a simplified method based on both experiments and analytical work was developed. This method enables the user to predict with reasonable accuracy the amount of change in fundamental frequency and stiffness that can be expected for a given damage situation. While this technique has not been extended to higher frequencies or to other stabilators, it could serve as the basis of a more detailed future study.

If additional investigations of a similar nature are attempted, it is recommended that considerable attention be given to the support conditions in both the experimental and analytical programs. In the current research effort, it was not possible to completely eliminate the rotation at the root of the stabilator, but estimates were made as to the amount of rotation existing. After correcting for this, the comparisons between experimental and analytical results were satisfactory.

LIST OF REFERENCES

1. Smith, J. H., "Nonlinear Beam and Plate Elements," Journal of the Structural Division, Proceedings of the American Society of Civil Engineers, March 1972.

2. Smith, J. H., "Analysis and Full-Scale Testing of Aircraft Shelters," AFWL-TR-70-170, Air Force Weapons Laboratory, Kirtland AFB, April 1971.

3. Smith, J. H., and Vann, W. P., "Theoretical and Experimental Investigation of Buried Concrete Structures," AFOSR-TR-1070 and AFATL-TR-76-55, November 1975.

4. Newmark, N. M., "A Method of Computation for Structural Dynamics," Proceedings ASCE, Vol. 85, No. EM3, 1959, pp. 67-94.

5. Bathe, K. J. and Wilson, E. L., "Stability and Accuracy Analysis of Direct Integration Methods," Journal of Earthquake Engineering and Structural Dynamics, Vol. 1, 1973, pp. 283-291.

6. Biggs, John M., Introduction to Structural Dynamics, McGraw-Hill Book Company, New York, 1964.

7. Boresi, A. P., Sidebottom, O. M., Seely, F. B., and Smith, J. O., Advanced Mechanics of Materials, John Wiley & Sons, New York, 1978.

8. Draper, N. R., and Smith, H., Applied Regression Analysis, John Wiley and Sons, New York, 1966.

UNCLASSIFIED
SECURITY CLASSIFICATION OF THIS PAGE (When Data Entered)

REPORT DOCUMENTATION PAGE	READ INSTRUCTIONS BEFORE COMPLETING FORM
1. REPORT NUMBER: AFOSR-TR- 78-1621	2. GOVT ACCESSION NO. / 3. RECIPIENT'S CATALOG NUMBER
4. TITLE (and Subtitle): DYNAMICS OF COMPLEX STRUCTURES - ANALYSIS AND EXPERIMENT: DAMAGED AIRCRAFT STABILATORS	5. TYPE OF REPORT & PERIOD COVERED: FINAL 15 JAN 1977 - 15 JUL 1978
	6. PERFORMING ORG. REPORT NUMBER
7. AUTHOR(s): JIMMY H. SMITH, W. LYNN BEASON	8. CONTRACT OR GRANT NUMBER(s): AFOSR 77-3231
9. PERFORMING ORGANIZATION NAME AND ADDRESS: TEXAS TECH UNIVERSITY, DEPARTMENT OF CIVIL ENGINEERING, LUBBOCK, TEXAS 79409	10. PROGRAM ELEMENT, PROJECT, TASK AREA & WORK UNIT NUMBERS: 2307B1, 61102F
11. CONTROLLING OFFICE NAME AND ADDRESS: AIR FORCE OFFICE OF SCIENTIFIC RESEARCH/NA, BUILDING 410, BOLLING AIR FORCE BASE, D.C. 20332	12. REPORT DATE: NOV 1978
	13. NUMBER OF PAGES: 80
14. MONITORING AGENCY NAME & ADDRESS(if different from Controlling Office)	15. SECURITY CLASS. (of this report): UNCLASSIFIED
	15a. DECLASSIFICATION/DOWNGRADING SCHEDULE

16. DISTRIBUTION STATEMENT (of this Report)

Approved for public release; distribution unlimited.

17. DISTRIBUTION STATEMENT (of the abstract entered in Block 20, if different from Report)

18. SUPPLEMENTARY NOTES

19. KEY WORDS (Continue on reverse side if necessary and identify by block number)

Dynamics
Damage
Stabilators
Regression Analysis
Experimental

20. ABSTRACT (Continue on reverse side if necessary and identify by block number)

This report presents the results of an experimental and analytical program employed to determine the effect that damage to a horizontal stabilator has on structural characteristics such as stiffness, natural frequencies and damping. A simplified method of computing the change in the fundamental frequency as damage increases is also developed.

DD FORM 1 JAN 73 1473 EDITION OF 1 NOV 65 IS OBSOLETE

UNCLASSIFIED
SECURITY CLASSIFICATION OF THIS PAGE (When Data Entered)